I-3a

Scientific Payloads

Anna Gregorio[1, 2, 3, 4]
[1]*Associate Professor, University of Trieste – Department of Physics, via Valerio, 2 – I 34127 Trieste, Italy*
[2]*Legal Representative, PICOSATS SRL, Padriciano, 99 c/o Area Science Park – I 34149 Trieste, Italy*
[3]*Associated to INFN – Istituto Nazionale di Fisica Nucleare, Trieste*
[4]*Associated to INAF – Istituto Nazionale di Astrofisica - Osservatorio Astronomico di Trieste*

1.1 Introduction

One major question for many Nanosatellite developer is, which kind of payloads can be accommodated on board those very small satellites. This question does not simply relate the feasibility of the measurement rather its quality, intended as the performance of the scientific results small satellites can produce. Some solutions are inhibited by strict technical limitations that will be hardly overcome in the next future, e.g. power and thermal control: Lidars, or sophisticated instruments for Astrophysics measurements.

If one does not consider the payloads excluded by these hard, technical limitations, the main point of nanosatellites is the size as payload performance often depends on its dimension especially for what regards scientific payloads. Here I take as a reference very small satellites as the CubeSats, a box of 10 cm cubic base and 30 cm length: a 3U CubeSats, although many of the instruments I'm going to describe are better fitting within a 6U CubeSat, but the general discussion does not change.

To start with, the performance of optical imaging systems for Earth observations (nadir pointing) are linked to the physical limitations on the aperture area size. If D is the aperture, h the altitude, Δx the ground spatial resolution, λ the reference wavelength and $\Delta\theta$ the angular resolution, then for a diffraction limited optical system:

$$\Delta x \approx h \cdot \Delta\theta \approx h \cdot 2.44 \cdot \lambda / D \tag{1.1}$$

By considering an average value of λ = 550 mm, an altitude of 600 km and an aperture of the order of 10 cm, the maximum achievable resolution is of the order of 5 meters.
Optical systems required to perform high quality imaging of distant astronomical objects and other sophisticated cosmological studies are surely another example since their sensitivity and signal to noise ratio (SNR), defined as the ratio between the detected signal S_{el} and the total noise N_{tot} in the measured wavelength band $\Delta\lambda$ depend on physical limitations of the collecting and aperture area D. There is not a unique recipe to estimate the SNR, a reasonable one is the following:

$$SNR = S_{el}/N_{tot} = S \cdot D \cdot \eta \cdot T_{exp} \Big/ \sqrt{(S + 2Bfov^2) \cdot D \cdot \eta \cdot T_{exp}} + 2N \cdot T_{exp} + 2R^2 \tag{1.2}$$

where T_{exp} is exposure time, FOV the system field of view, η the total receiver efficiency, B the contribution coming from the background (the light coming from the sky itself), N the thermal noise and R the read-out noise.

In an analogous way, the physical size of small satellites prevents the implementation of high-performance RF based systems (imaging radars, radar altimeters, lidars or even Synthetic Aperture Radars – SAR) limiting the gain G of the antenna and as a consequence the SNR:

$$\boldsymbol{G \approx \eta \cdot (\pi D/\lambda)^2} \tag{1.3}$$

where η is the antenna efficiency, of the order of 0.55. To design a high gain antenna, the antenna size shall be of the same order of the wavelength, for D being 10 cm, this corresponds to a 3 GHz radar system working in the C-band, while scientifically the most interesting bands stay at higher frequencies, e.g. in the 94 GHz band for weather forecasting or at multiple frequencies.

These types of scientific programs are mostly out of the scopes of small satellites, although some efforts are being carried on and interesting results are being achieved.

1.2 Categorisation

Before starting dealing with the proper payload description and analysis, it is worth analysing the type and purpose of **science missions**. For small satellites, the mission categorisation is not that different from the most general case [1]:

- **Earth Observation**. These missions are dedicated to the Earth Observation to understand how the global Earth system is changing and what are the sources of change in the Earth system and their magnitude and trends.
- **Solar and Space Weather**. Sun and near-Earth environment observation: corona, magnetic field, solar wind, Earth atmosphere and magnetosphere, etc.
- **Planetary**. These missions may resemble the Earth Observation type missions, but they relate to the other Solar System planets and might include landers and eventually rovers.
- **Astronomy**. These missions concern with measuring far-away bodies such as galaxies, stars and exo-planets.
- **Astrophysics & Fundamental Physics and Biology**. Astrophysics & Fundamental Physics missions concern mostly with the observation of deep space, a branch of astronomy that studies the physical laws, the properties and dynamic processes of celestial bodies and of the Universe, and their evolution. Biology missions concern with the observation of the effect of the harsh space environment on biological systems.

The table below gives a clear representation of the number and applications of CubeSat missions launched or under development by NASA and NSF in these scientific fields [1], Figure Error! No text of specified style in document.**.1** the application trend.

Table Error! No text of specified style in document.**.1** Summary of CubeSat Statistics for NASA and NSF (NAP report [1])

Launch Dates	Technology	Astronomy & Astrophysics	Biological & Physical Science	Earth Science	Solar and Space Physics	Planetary Science	Total
2006-2015	28	0	4	1	14	0	47
Planned 2016-2018	32	1	4	7	10	3	57
Total	60	1	8	8	24	3	104

In the following sections I will briefly discuss the typical scientific objectives for each of these categories and discuss the payloads that have been conceived to meet these requirements by using small satellites. The number of CubeSat missions is rapidly increasing and is not feasible to discuss all the scientific payloads. Only the most recent payloads, grouped by type, or most representative concepts will be proposed.

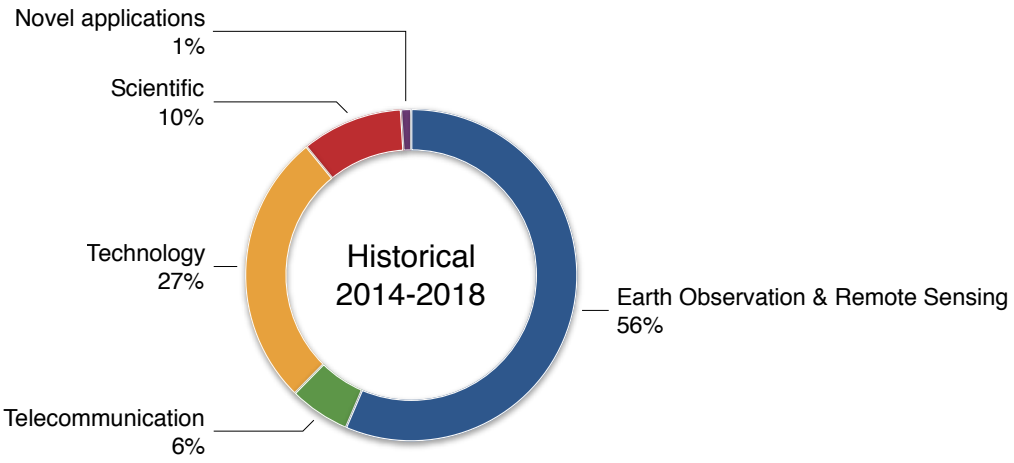

Figure Error! No text of specified style in document.**.1** Small satellite (1-50 kg) application trend, 2019 market forecast by Spaceworks Enterprises Inc.

It has to be stressed that in order to perform this review, five sources of information are considered crucial and have been used along this document, namely:

1. The NAP report "Achieving Science with CubeSats: Thinking Inside the Box" [1];
2. The EO Portal Satellite Missions Database, available on https://directory.eoportal.org/ [2];
3. IDA - Global Trends in Small Satellites [3];
4. NATIONAL SCIENCE FOUNDATION (NSF), Cubesat-Based Science Missions For Geospace And Atmospheric Research, October 2013 [4];
5. Gunter's Space Page, URL: http://space.skyrocket.de/ [5].

1.3 Imagers

An imager detects and conveys the information that constitutes an image, in a defined wavelength band. Optical imagers provide images, typically of Earth surface and atmosphere, and represent the most common instruments used for Earth observation and the most common payload for CubeSat small satellites. According to [1], in 2014 71% of US CubeSat launches were Earth-imaging CubeSats. They are generally nadir-viewing instruments.

1.3.1 MCubed-2 / COVE

As a representative optical imagining payload for Earth observation, the COVE (CubeSat On-board processing Validation Experiment) instrument on board the MCubed-2 developed by the UM (University of Michigan), aims at producing color images of the Earth by using an OmniVision 2 Mpixel CMOS camera chip (OV2655) from a LEO at a resolution better than 200 m [2,6,7].

The camera, also referred to as µEye, has a 9.6 mm EFL (Effective Focal Length) Plano-convex lens, images are saved to a Colibri PXA270 microprocessor at a resolution of 1280×1024 pixels, with a pixel size of 3.6 µm × 3.6 µm. This allows for moderate to high-resolution images of the Earth after post-processing. The whole camera payload subsystem is fairly small with only 55 cm^3 of volume [8].

1.3.2 SwissCube

The objective of SwissCube is to perform spaceborne observations of the airglow occurring in the upper atmosphere at an altitude of about 100 km. The telescope consists of a PCB (Printed Circuit Board), including a detector and its control electronics, and an optical system, comprising a baffle, the band pass filter which selects the desired wavelength of the oxygen emissions and focusing optics [2,9,10].

The optical system has a size of 30 mm × 30 mm × 65 mm, the payload board 80 mm (length) × 35 mm (width) × 15 mm (depth); the total mass is 50 g. A CMOS detector is used for photon detection, with a FOV of 18.8º×25º and a resolution of 0.16º/pixel. The payload consumes 450 mW during 30 s for each image capturing.

In order to avoid straylight, the payload is mounted to one of the sides of the satellite via a baffle as shown in Figure Error! No text of specified style in document..**2**.

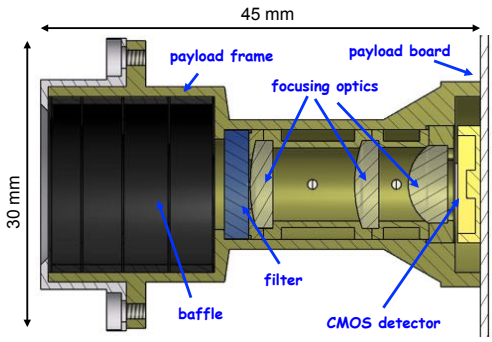

Element(s)	Material	Mass
Closing cap	Aluminium	3 g
Payload frame	Titanium	20 g
Vanes	Stainless steel	2 g
Spacers for the baffle	Aluminium	2 g
Spacers for the optics	Titanium	4 g
Lenses	Glass (BK 7)	1 g
Filter	Glass (RG 9)	1 g
Payload board	PCB	15 g
Screws	Stainless steel	2 g
Total mass		**50 g**

Figure Error! No text of specified style in document..**2** Cross-section of the telescope its elements and mass budget (image credit & copyright: EPFL).

In a first phase of three months, airglow emissions are observed at different regions and under different angles of observation. These measurements are required to evaluate minimum, maximum and mean intensities of airglow emissions during both day and night and to analyze the background radiation due to scattered sun or moonlight. In a second phase only, observations of airglow emissions at limb between 50 and 120 km are carried out to study more carefully their variation in intensity.

1.3.3 AARest

AAReST (Autonomous Assembly of a Reconfigurable Space Telescope**)** goal is to demonstrate all key technological aspects of autonomous assembly and reconfiguration of a space telescope based on an optical focal plane assembly (camera) and multiple mirror elements synthesizing a single coherent aperture [2,11].

The stowed volume of the telescope is 0.5 m × 0.5 m × 0.6 m. After separation from the primary payload, the telescope deploys its sensor package to the focus of the mirror array using a mast. Figure Error! No text of specified style in document..**3** depicts the components of AAReST: "Coresat", 2 separate "MirrorCraft", a camera package and a deployable boom [12].

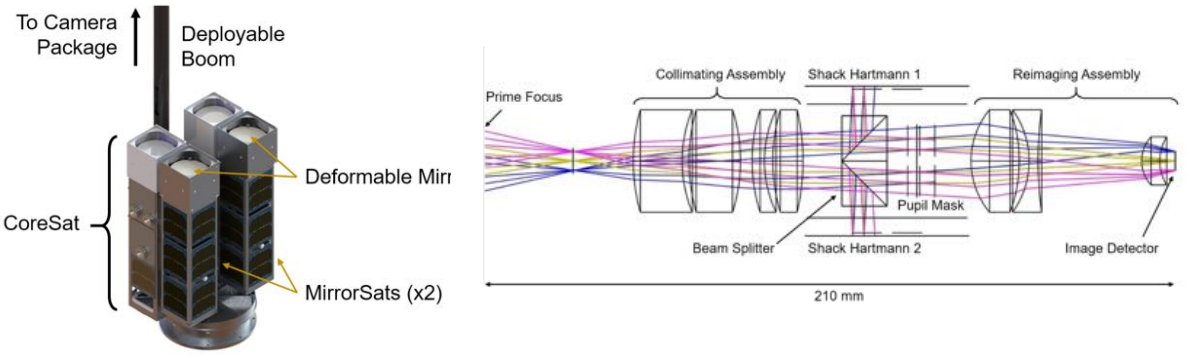

Figure Error! No text of specified style in document..**3**: Left: AAReST spacecraft components. Right: Geometric ray-trace of the optical path within the Camera Package (image credit: JPL and Caltech/SSL)

The camera package, located at the focus of the telescope, contains various elements such as corrective optics, wave front sensors and an imaging detector. Light originating from the prime focus of the telescope enters the camera and is passed through a series of collimating lenses. A pair of beam splitters redirect a portion of this light onto two Shack Hartmann wave front sensors providing the shape of the deformable mirrors. The remaining beam travels through a pupil mask and a set of lenses to re-image the light onto the imaging detector. Images are captured using this after a calibration process.

The MirrorCrafts are independent spacecraft used to house the deformable mirrors, sit atop these spacecraft. Each MirrorCraft is equipped with its own propulsion system to perform the autonomous reconfiguration and docking maneuvers by using electromagnets and a computer vision system. The deformable mirrors are made

using thin glass wafers and a layer of piezoelectric polymer. A custom electrode pattern is incorporated onto the backside of the piezoelectric polymer allowing for shape control to be performed. The mirrors have a total stroke of ~40 μm, allowing for the correction of large shape errors [13].

1.4 X-Ray Detectors

X-Ray detection cannot be performed by using standard optical system but on small satellites, due to size limitations, nor even by using grazing incident systems. Rather particle detection systems typically based on silicon sensors are employed.

Quite often small satellites use Silicon Drift Detectors (SDDs), able to detect both hard and soft X-ray photons. SDDs are small and work at low voltage, making them perfectly fit to miniaturized spacecrafts. Electrons are generated by the photon impinging on the SDD, drifted towards and finally collected by the anodes; SDDs can measure the energy of the incoming photon by counting the amount of electrons it produces. At room temperature SDDs offer an extremely low noise level.

1.4.1 MinXSS

MinXSS (Miniature X-ray Solar Spectrometer) [14,15] is a 3U CubeSat solar physics mission of the UC (University of Colorado), designed to better understand the energy distribution of solar flare SXR (Soft X-ray) emissions and its impact on the Earth ITM (Ionosphere, Thermosphere, and Mesosphere). MinXSS, measurements of the solar SXR irradiance will provide a more complete understanding of flare variability in conjunction with measurements from RHESSI and SDO EUV Variability Experiment (EVE).

MinXSS science measurements will be achieved using the commercially available X123-SDD advanced X-ray spectrometer of Amptek [18], with an active area of 25 mm^2, an effective Si thickness of 0.5 mm, an 8 μm thick Be filter on the detector vacuum housing, an active two stage TEC (Thermoelectric Cooler) on the detector, and sophisticated MCA (Multichannel Analyzer) detector electronics. Key to achieving MinXSS science goals is accurate pointing control and knowledge: with the wide field of view of ±4°, the pointing requirements are 2° (3σ) accuracy and 0.05° (3σ) knowledge. Finally, MinXSS observes the soft X-ray solar spectrum from about 1 keV to 5 keV, with a resolution better than 0.5 keV and accuracy better than 30%.

1.4.2 HALOSAT

HaloSat (Soft X-ray Surveyor) is a NASA 6U CubeSat astronomical science mission aimed at measuring soft X-ray emissions from the halo of the Milky Way galaxy and contribute to solve the "missing baryon" problem looking at hot halos surrounding galaxies [2,16,17].

Also, HaloSat uses SDDs from Amptek Inc. [18] with an active area of 25 mm^2 behind a Si_3N_4 window, testing shows ΔE ~80 eV FWHM at 451 eV. The SDDs view the sky through a 13.3 mm diameter hole that is 135 mm away (9.2º - 13.4º). The detector is enclosed in a scintillator readout with APDs (Avalanche Photo Diodes) to reject charged particle background, see figure below.

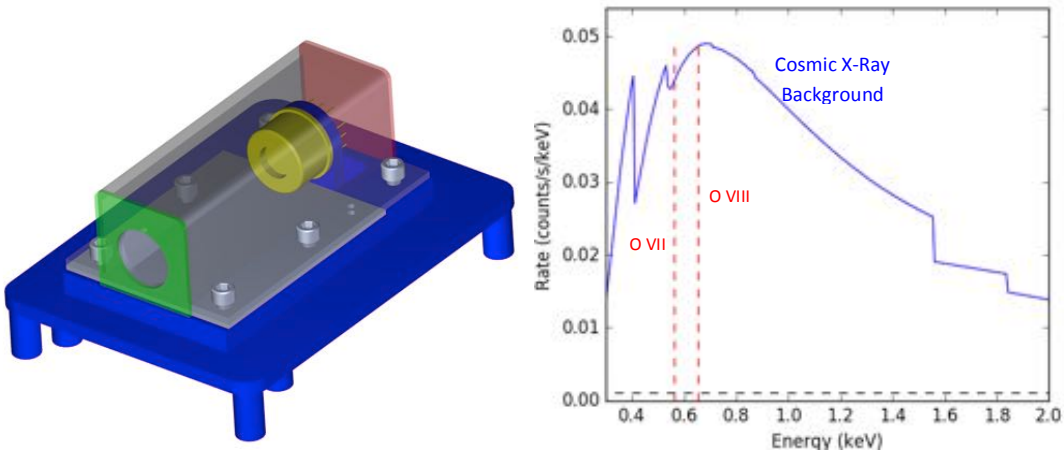

Figure Error! No text of specified style in document.**.4:** Sensor assembly: SDD detector surrounded by a Copper-Tungsten alloy shielding (image credit: University of Iowa)

1.4.3 HERMES

Another interesting example is the new European mission HERMES (High Energy Rapid Modular Ensemble of Satellites) – a space-based instrument for high energy (keV-MeV) astrophysics, a science domain previously limited to large space missions. HERMES consists of a constellation of modular nanosatellites in low Earth orbit, equipped with X-ray detectors, again an SDD designed on purpose, with at least 50 cm^2 of active collecting area in the broad band between a few keV and ~1 MeV each, and very high time resolution (μs). The main science goal is to study and accurately localize high energy astrophysical phenomena such as Gamma-Ray Bursts, possible electromagnetic counterparts of gravitational waves, and the potential high-energy counterparts of Fast Radio Bursts. The transient localization is achieved through triangulations, by measuring the delay of signal arrival time on different nanosatellites, due to the very high temporal resolution of individual detectors.

1.4.4 CXBN

The goal of the CXBN (Cosmic X-ray Background Nanosatellite) science missions is to significantly increase the X-ray measurement precision in the 30-50 keV range, where the diffuse cosmic X-ray background peaks in order to constrain models that attempt to explain the relative contribution of X-ray sources. Results from the mission will lend insight into the underlying physics of this phenomenon [2,19,20].

The CZT (Cadmium Zinc Telluride) array is the CXBN science instrument (or science array), developed by Redlen Technologies. The manufacturing process known as the Traveling Heater Method (THM) allows an extremely uniform crystalline structure in the semiconductor material so that charge is evenly distributed, finally improving the energy resolution. The imaging module is formed by 2 × 2 array of 64-pixel CZT detectors with thicknesses of 5 mm and 2.46 mm pixel pitch, bonded to a common cathode plate.

1.4.5 MiSolFA

The Micro Solar-Flare Apparatus (MiSolFA) [21] goal is to provide key insights into the evolution of the solar magnetic field by using a scaled-down version of the HMI (Helioseismic and Magnetic Imager) developed for the European Space Agency's (ESA's) Solar Orbiter mission, to be installed into a 6-unit platform.

MiSolFA exploits indirect imaging techniques to provide independent spectra for different sources in the field of view, or to provide images in different energy ranges, achieving 10 arcsec = 0.003° angular resolution. With longer distance between front and rear grids and/or by adopting smaller slit periods, the angular resolution can become better than 1 arcsec. This will make it possible to measure the size of the chromospheric sources and compare them against the EUV "ribbons", and to study the source height dependence on the photon energy.

Viewed from the Sun, the first instrument unit is the Imager, sitting just behind a passive thermal shield, which transmits only X-rays above about 5 keV, and hosting the Aspect System, which precisely determines the Sun location inside the FOV of the imager. A pair of parallel grids is placed in front of a photon detector, the grids

and the detector form a “subcollimator”, which provides information about one Fourier component of the image (two real values). The imager produces moiré patterns, see Figure Error! No text of specified style in document..**5**, on photon detectors, enclosed in the Detector Box. The moiré pattern is sensitive to the source location along one direction (orthogonal to the slits); two point-like sources displaced along this direction will produce similar modulation patterns, but with different phase. Data from them and from the Aspect System are collected by a system logically subdivided into two units, the Detector Interface Unit (NASA) and the Data Processing Unit.

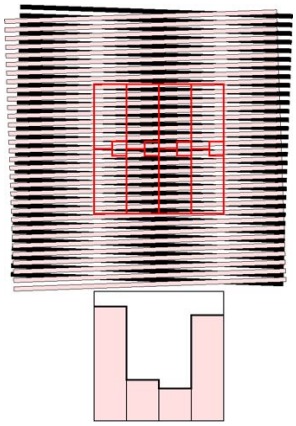

Figure Error! No text of specified style in document..**5**: Subcollimator response to point-like source. A minimum of 4 pixels spanning one moiré period is required to reconstruct amplitude and phase of the modulation [21].

The amplitude of the modulation, or equivalently the contrast of the moiré image, changes as a function of the source size, the maximum amplitude is obtained with a point-like source. A set of sub-collimators sampling different angular scales along independent directions is required to mathematically reconstruct an image of the X-ray emitting source.

1.5 Spectrometers

Spectrometers measure a spectrum, typically the flux intensity as a function of wavelength, of frequency, of energy, of momentum, or of mass.

1.5.1 SOLSTICE

The SOlar Stellar Irradiance Comparison Experiment (SOLSTICE) [2,22,23] is one of four solar irradiance measurement experiments launched as part of the Solar Radiation and Climate Experiment (SORCE) in 2003. The mission aims at producing daily solar UV irradiance measurements, comparing them to the irradiance from an ensemble of 18 stable early-type bright blue stars serving as monitor of instrument calibration.

SOLSTICE is a two-channel grating spectrometer aimed at measuring UV radiation in the spectral coverage of 115 to 320 nm with a spectral resolution between 0.1 nm and 0.2 nm. The instrument is made of two identical spectrometers, mounted at right angles to facilitate verification of stellar pointing. A mirror reflects the beam on one of two diffraction gratings mounted on a gimbal; rotating the gimbal causes the diffraction of a small wavelength band toward a second plane mirror. The grating disperses the radiation and directs a specific wavelength onto one of the two photomultiplier detectors.

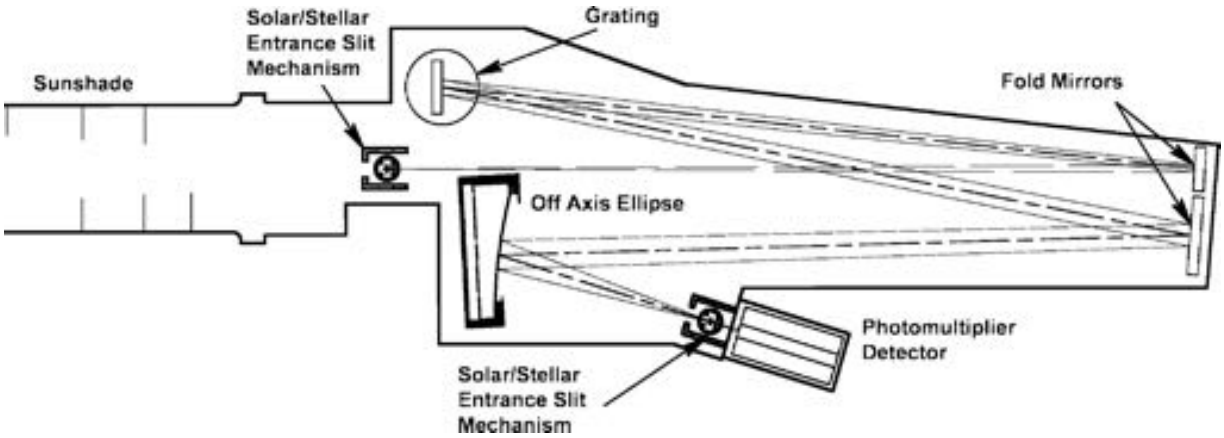

Figure Error! No text of specified style in document.**.6**: Optical-mechanical configuration of a single SOLSTICE I channel (image credit: Laboratory for Atmospheric and Space Physics - LASP) [22]

The Compact Solstice (CSOL) inherits the SOLSTICE experience for future developments of FUV/MUV CubeSat-sized instruments, still in the full 110-300 nm spectral range on a 10 s cadence, for routine monitoring of solar irradiance. CSOL occupies about 10% the volume of the SORCE SOLSTICE and provides the same wavelength coverage.

LASP is also making a miniature version of the SORCE Solar Irradiance Monitor for nanosatellites.

1.5.2 OPAL

The OPAL (Oxygen Photometry of the Atmospheric Limb) [2,24,25] goal is to analyze the thermospheric temperature signals of the dynamic solar, geomagnetic, and internal atmospheric forcing by remote sensing of the altitude temperature from the atmospheric limb from a mid- to high-inclination orbit (>50º).

The OPAL instrument is a high-resolution imaging spectrometer that simultaneously collects spatially-resolved A-band spectra in multiple azimuthal directions and across the full altitude range of A-band emission. The neutral temperature can be estimated from the qualitative shape of the A-band spectrum over the range 150-1500 K [26]: as the temperature increases, the relative intensity of the R branch (759-762 nm) increases and shifts to shorter wavelength while the P branch (762-770 nm) widens and shifts to longer wavelength.

OPAL is a grating-based imaging spectrometer with refractive optics and a high-efficiency VHG (Volume Holographic Grating). The optical path is folded into three legs, each about 80 mm long. The scene is sampled by 7 parallel slits that form non-overlapping spectral profiles at the focal plane with a resolution of 0.5 nm (spectral), 1.5 km (limb profiling), and 60 km (horizontal sampling).

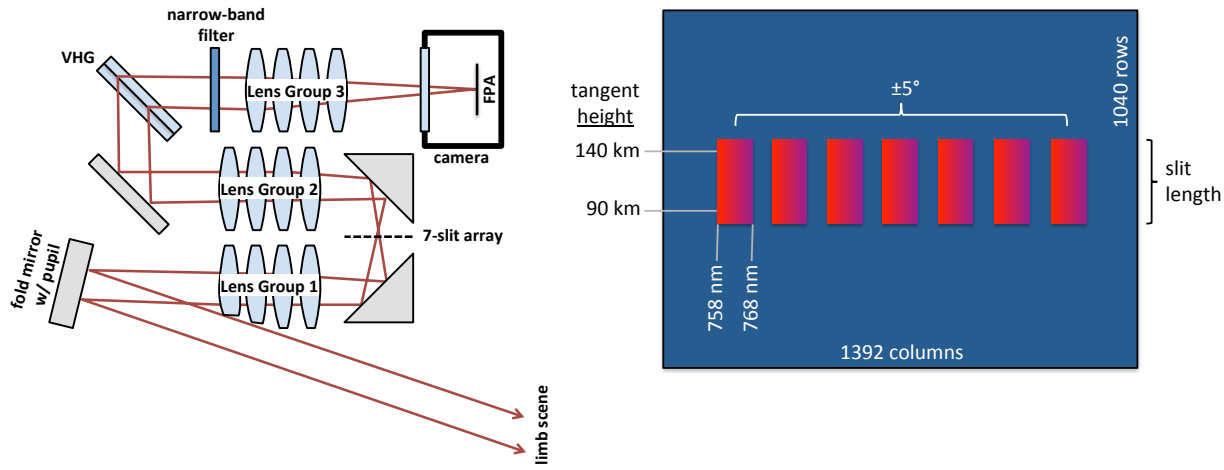

Figure Error! No text of specified style in document.**.7**: Left: Schematic view of the spectrometer optics (image

credit: USU/SDL) and light path. Light from the limb scene enters the instrument via a front fold mirror, coincident with the entrance pupil; the scene is imaged onto the slit array by a 4-element lens assembly (group 1); light through the slits is recollimated by another 4-element lens assembly (group 2, identical to the first); light is then dispersed along an axis perpendicular to the slits by the VHG aligned to the Littrow condition (incidence angle ~ diffraction angle); a narrow-band filter selects A-band wavelengths and finally the last four-element lens assembly (group 3) reimages the slits onto the FPA. Right: Focal plane utilization, dispersion is less than spacing between slit images to avoid spectra overlapping (image credit: USU/SDL).

The OPAL spectrometer is entirely comprised of COTS components, except for the band pass filter and VHG, which are inexpensive semi-custom elements. The low noise and high sensitivity CCD camera, is model Trius SX9 from Starlight Xpress, the sensor is a Sony ICX285AL monochrome CCD with 1392×1040 pixels at a 6.45 µm pitch. The photon detection efficiency in the A-band is 32%. The camera provides 16-bit readout over a USB interface with RMS readout noise of only 5 e^-. The ultra-low dark current (0.1 e^-/s/pixel at 10ºC) supports the extended exposure necessary to observe the A-band emissions.

1.5.3 Lunar IceCube / BIRCHES

The primary objective for the Lunar IceCube mission [2,27,28] is to prospect for water in solid, liquid and vapour forms, while also detecting other lunar volatiles. The mission is designed to address existing strategic knowledge gaps related to lunar volatile distribution, focusing on the abundance, location and transportation physics of water ice on the lunar surface at a variety of latitudes. The required scientific observations will be performed from a highly-inclined, low-periapsis, elliptical lunar orbit using the Broadband InfraRed Compact High-Resolution Exploration Spectrometer (BIRCHES). A footprint of 10 km from a lunar altitude of 100 km is a key mission requirement, footprint of 10 km in track-direction regardless of altitude, larger in cross-track direction above 250 km.

BIRCHES is a miniaturized version of OVIRS on OSIRIS-Rex, a compact spectrometer (1.5U, 2.5 kg, 10-15 W) with a compact cryocooled HgCdTe focal plane array (Teledyne H1RG) for broadband (1 to 4 µm) measurements, achieving sufficient SNR (>400) and spectral resolution (10 nm) through the use of a Linear Variable Filter (LVF) to characterize and distinguish important volatiles (water, H_2S, NH_3, CO_2, CH_4, OH, organics) and mineral bands. The instrument has built-in flexibility, using an adjustable 4-sided iris, to maintain the same spot size regardless of variations in altitude (by up to a factor of 5) or to vary spot size at a given altitude, as the application requires. Also, electronics can be reconfigured to support the instrument in ‘imager' mode. Thermal design is critical for the instrument: a compact and efficient cryocooler is designed to maintain the detector temperature below 120 K. In order to maintain the optical system below 220 K, a special radiator is dedicated to optics alone, in addition to a smaller radiator to maintain a nominal environment for spacecraft electronics.

1.5.4 GRIFEX

The GEO-CAPE ROIC In-Flight Performance Experiment (GRIFEX) [2,29,30,31] is a 3U CubeSat mission dedicated to measurements of rapidly changing atmospheric chemistry and pollution transport with the Panchromatic Fourier Transform Spectrometer (PanFTS) instrument. The aim is also to perform engineering assessment of a JPL-developed all digital in-pixel high frame rate Read-Out Integrated Circuit (ROIC), constituting the focal plane assembly, and to validate detector technology for the PanFTS.

In this context the ROIC works with the PanFTS, a key component of the interferometer used for high-resolution measurements (temporal, spatial, and spectral) to capture rapidly evolving tropospheric chemistry from geostationary orbit on an hourly basis. The PanFTS design [32] combines a conventional Michelson interferometer with a number of features based on spectrometers like TES (Tropospheric Emission Spectrometer) to measure thermal emission, like OCO (Orbiting Carbon Observatory) and OMI (Ozone Monitoring Instrument) to measure scattered solar radiation. The design has two parallel optical trains, see Figure Error! No text of specified style in document..**8** (right) one for infrared wavelengths and one for UV-Vis. The beam aperture of 5 cm is driven by the Rayleigh criterion to resolve the ground pixels. The instrument temperature is 180 K to minimize instrument self-emission.

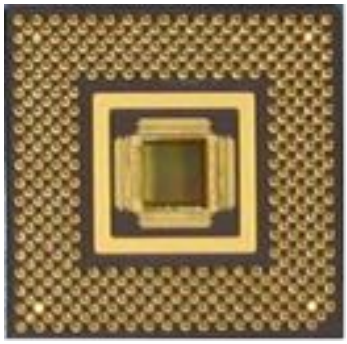

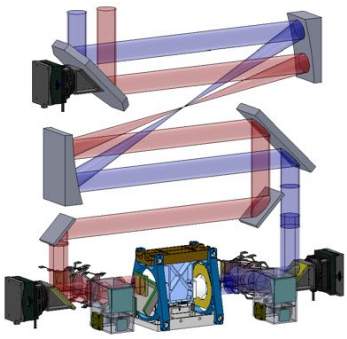

Figure Error! No text of specified style in document..**8**: Left: ROIC/FPA design: 128 × 128 array, 60 µm pixel. Right: the PanFTS Engineering Model [32] (image credit: NASA/JPL and U. Michigan)

1.5.5 HyperCube

A similar concept of the one used by GRIFEX applies to HyperCube [2,33,34], a constellation of 6U CubeSats equipped with MWIR (Mid-Wave Infrared) hyperspectral instruments for Earth Observations to measure three-dimensional distributions of atmospheric water vapor. HyperCube wants to infer wind velocities at multiple vertical locations in the atmosphere by measuring the same region of the atmosphere at different times.

The instrument contains an FTS-based hyperspectral sounder, a cross-track step-stare scanner, a compact telescope, an IR FPA and a calibration source. The scanner performs step-stares, the Earth radiance arrives to the scanner, enters the Michelson interferometer creating the interferogram that is finally acquired by the FPA.

1.6 Photometers

Photometry measures the flux, or intensity, of an object light.

1.6.1 XPS

XPS (XUV Photometer System) [2,35,36] is one of the payloads of the SORCE mission, heritage of SNOE and of the SEE (Solar EUV Experiment) instrument on the TIMED mission. The XPS objective is to measure the XUV (Extreme Ultraviolet) solar irradiance from 1 to 35 nm. The instrument package is a set of filter photometers consisting of 12 silicon XUV photodiodes. Each photodiode has a thin-film filter to provide an approximately 5 nm spectral band pass. These thin film filters are deposited directly on the photodiode to avoid using delicate metal foil filters which are difficult to handle, prone to develop pin holes, and degrade with time. The set of twelve XUV photometers is packaged together with a common filter wheel mechanism, which can rotate a closed aperture, a fused silica window, or an open aperture in front of any given photometer. The fused silica windows on this filter wheel allow accurate subtraction of the background signal from visible and near UV light. The 12 XUV photometers (XPs) are grouped into three sets. Each set of four XPs is arranged in a circle for use with the filter wheel mechanism. The filter wheel, which has three different rings of filters for the three sets of XPs, has eight positions: four blocked for dark measurements, two clear for solar XUV measurements, and two with fused silica windows for solar visible background measurements. An observation run is a sequence of measurements from five consecutive filter wheel positions, normally starting and ending with dark measurements. The electronics for each photodiode include only a current amplifier and a voltage-to-frequency (VTF) converter.

1.6.2 BRITE - Photometer

The objective of BRITE (BRIght-star Target Explorer) [2,37,38] is to examine the apparently brightest stars in the sky for variability using the technique of precise differential photometry in time scales of hours and more. The constellation of four nanosatellites is divided into two pairs, with each member of a pair having a different

optical filter. The requirements call for observation of a region of interest by each nanosatellite in the constellation for up to 100 days or longer.

The science payload of each nanosatellite consists of a five-lens telescope with an aperture of 30 mm and the interline transfer progressive scan CCD detector KAI 11002-M from Kodak with 11 M pixels. A baffle is used to reduce stray light. The optical elements are housed inside the optical cell and are held in place by spacers. The photometer has a resolution of 26.52 arcsec/pixel and a field-of-view of 24º. The mechanical design for the blue and for the red instrument is nearly identical, only lenses size is different.

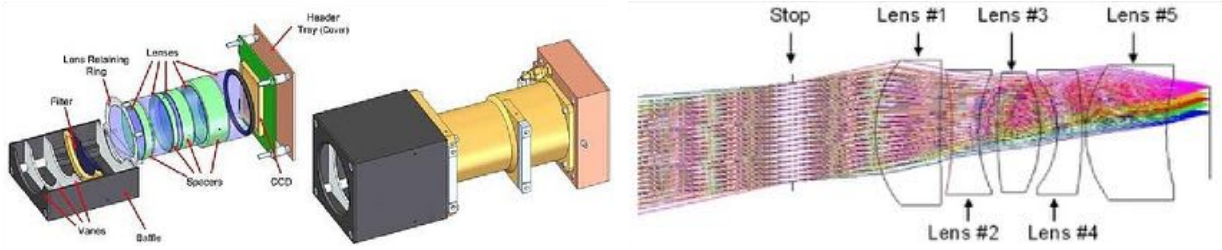

Figure Error! No text of specified style in document.**.9**: Left: illustration of the BRITE telescope and baffle (image credit: UTIAS/SFL). Right: the optical design of the photometer (image credit: UTIAS/SFL, Ceravolo)

The effective wavelength range of the instrument is limited in the red (550-700 nm) by the sensitivity of the detector and in the blue (390-460nm) by the transmission properties of the glass used for the lenses. The filters were designed such that for a star of 10,000 K (average temperature of target stars) both filters would generate the same amount of signal on the detector.

1.6.3 ExoPlanet & ASTERIA

The objective of ExoPlanet [2,39,40,41] is to verify the capability of small satellite to search for unmapped planets and to complement existing planet-hunters. During the diurnal phase, the spacecraft points the solar panels toward the Sun while during the eclipse, it slews to re-acquire the target star. The operation concept is shown in Figure Error! No text of specified style in document.**.10**. An Earth-twin transit across the center of a star would last 13 hours from a low inclination LEO, sufficient to detect such an event. The optimum integration time is a function of target star brightness and image size. The maximum integration time is on the order of 30 s.

The photon collection capability is a primary consideration given the photometric nature of the mission, this implies a large aperture (i.e. low f-number) lenses. The payload is a Zeiss 85 mm f/1.4 SLR (Single Lens Reflex) camera with an aperture of 60 mm along with CCD (1k×1k with 13.3 µm pixels, back-illuminated, 2 e- rms read noise, 12.5 e^-/pixel/s dark current at 0ºC and 12.5º diagonal FOV) and co-mounted CMOS detectors for star tracking (2.6k×1.9k with 1.3 µm pixels).

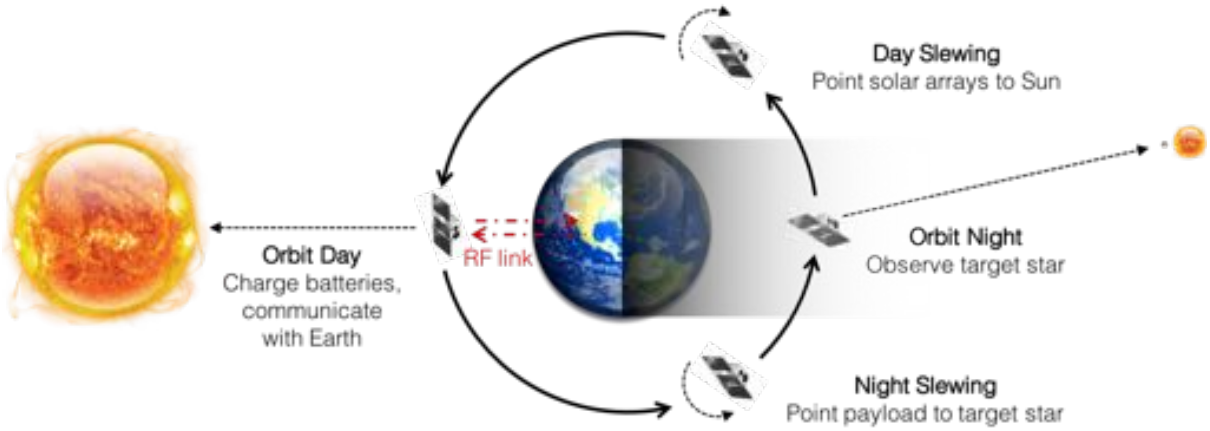

Figure Error! No text of specified style in document.**.10**: ExoPlanet operation concept [41] (image credit: NASA/JPL).

ExoPlanet has finally evolved into ASTERIA (Arcsecond Space Telescope Enabling Research in Astrophysics) [2,42] capable to achieve arcsec-level line of sight pointing error with highly stable focal plane temperature control. These technologies will enable careful measurement of stellar brightness over time.

The sensor suite includes an optics section, a dual-imager focal plane array realizing the two payload functions and a piezoelectric nano-positioning stage capable of moving the focal plane to zero-out the platform jitter.

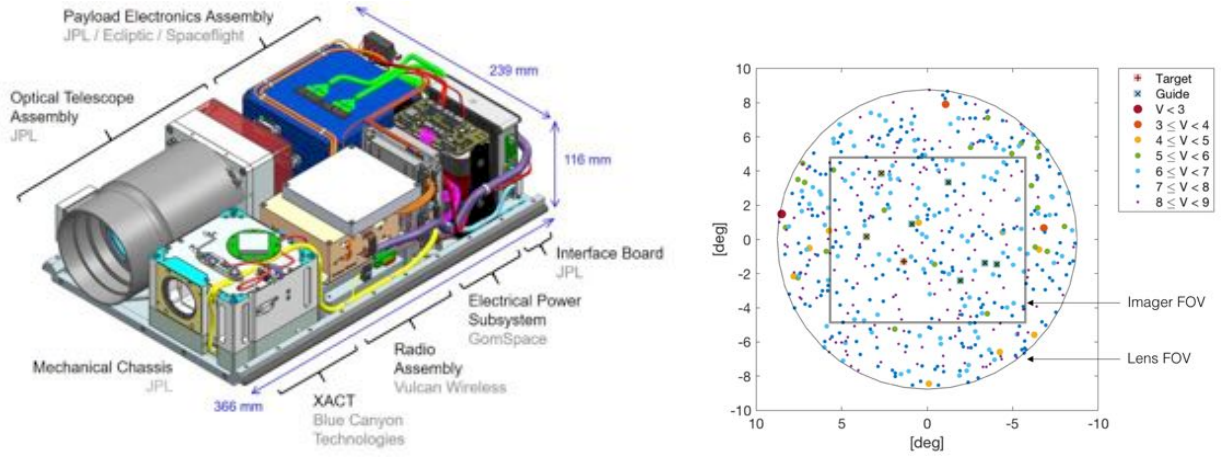

Figure Error! No text of specified style in document.**.11**: Left: illustration of the ASTERIA spacecraft, and, right, its starfield [42] (image credit: NASA/JPL, MIT).

The optics system is a f 1.4/85 Zeiss lens with a 28.6º FOV, focusing an image 43 mm in diameter onto the focal plane. The focal plane array houses two active detector areas, one larger CMOS detector that fulfills the science function and a smaller CMOS sensor with smaller pixel sizes to act as a rapid-cadence star camera to provide attitude information to the attitude control system. The science sensor operates at longer integration times and collects data on several pixel windows, one for the target star and several other bright stars for comparison plus dark areas of the sky for dark current correction.

1.7 GNSS Receivers

Small satellites can provide atmospheric measurements on a global scale and data for weather and climate forecasting. One of the techniques is based on existing global navigation satellite system-radio occultation (GNSS-RO), a precise and cost-effective technique for measuring Earth atmosphere from space. The understanding of many Earth processes benefits from this kind of observation, including severe weather, cloud formation and evolutionary processes, aerosols or air quality related measurements, atmospheric photochemistry,

vegetation, ocean color, solar irradiance and Earth outgoing radiation. CubeSat-enabled constellations could deliver tens of thousands of occultations daily and make them available in near real time [43].
The CYGNSS receiver is chosen here as the reference instrument, but also Spire, GeoOptics, and PlanetIQ are developing CubeSat-based GNSS-RO constellations. Also, the Constellation Observing System for Meteorology, Ionosphere, and Climate (COSMIC) mission is another constellation of microsatellites making atmospheric soundings of temperature, moisture, and pressure in the troposphere and stratosphere using GNSS-RO.

1.7.1 CYGNSS

Cyclone Global Navigation Satellite System (CYGNSS) [2,44,45] Earth Venture mission is complementary to traditional spacecraft that measure winds. By going from active to passive technology using GPS, CYGNSS requires significantly less power than does a spacecraft using the traditional technique. CYGNSS is a constellation of eight low Earth-orbiting spacecraft that analyze reflected GPS signals from water surfaces shaped by hurricane-associated winds.
Each CYGNSS spacecraft carries a delay-Doppler mapping instrument consisting of a multi-channel GPS receiver, low-gain zenith antennas, and high-gain nadir antenna. CYGNSS measures the ocean surface wind field associated with tropical cyclones by combining the all-weather performance of GPS-based bistatic scatterometry. The working principle is schematically shown in Figure Error! No text of specified style in document.**.12**.

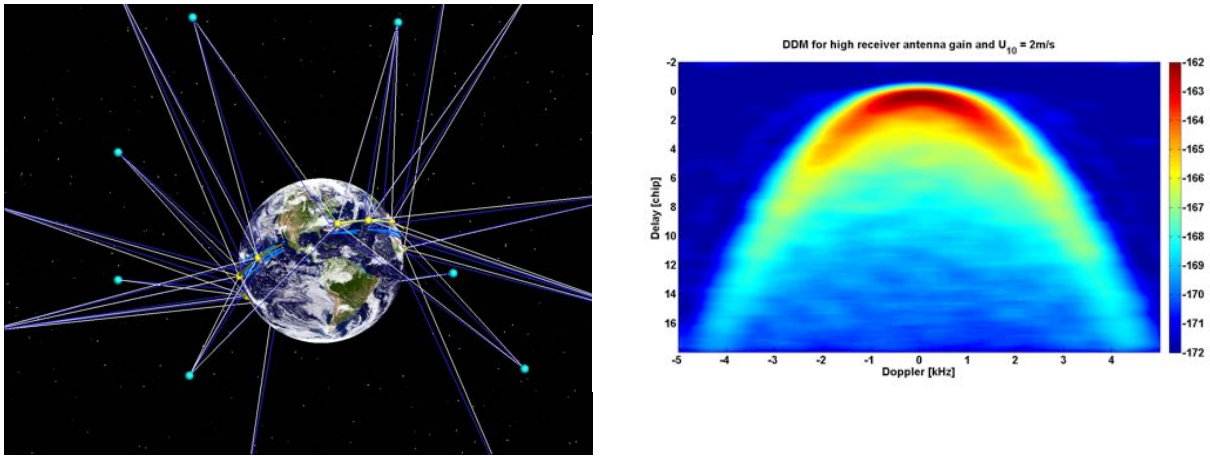

Figure Error! No text of specified style in document.**.12**: Left [2]: CYGNSS spacecrafts (yellow dots) analyze reflected GPS signals (dark blue lines) from water surfaces shaped by hurricane-associated winds. Red lines indicate signals directly between the CYGNSS satellites and the GPS satellites (light blue dots further from Earth). Blue lines on the Earth surface represent measurements of the wind speed that CYGNSS derives from the reflected GPS signal. Courtesy of NASA/University of Michigan. Right: Spatial distribution of the ocean surface scattering measured by the UK-DMC-1 demonstration spaceborne mission – referred to as the Delay Doppler Map (image credit: SSTL)

Figure Error! No text of specified style in document.**.12** illustrates the working principle. The direct GPS signal is transmitted from the orbiting GPS satellite and received by a RHCP (Right-Hand Circular Polarization) receive antenna on the zenith (i.e., top) side of the spacecraft that provides a coherent reference for the coded GPS transmit signal. The quasi-specular, forward-scattered signal that returns from the ocean surface is received by a nadir- (i.e., downward-) looking LHCP (Left-Hand Circular Polarization) antenna on the nadir side of the spacecraft. The scattered signal contains detailed information about its roughness statistics, from which the local wind speed can be derived.
The image on the right of Figure Error! No text of specified style in document.**.12** shows the scattering cross section and demonstrates its ability to resolve the spatial distribution of ocean surface roughness. This type of scattering image is referred to as a DDM (Delay Doppler Map). There are two different ways to estimate ocean surface roughness and near-surface wind speed from a DDM. The maximum scattering cross-section (the darkest region) can be related to roughness and wind speed [46] but this requires absolute calibration of the DDM, not always available. Another technique estimates wind speed from a relatively calibrated DDM using the shape of the scattering arc (the lighter shades). The arc represents the departure of the bistatic scattering from the theoretical purely specular case, a perfectly flat ocean surface, which appears in the DDM as a single-

point scatterer. This second approach relaxes requirements on instrument calibration and stability, however it uses a wider region of the ocean surface; this implies a lower spatial resolution.

1.7.2 CADRE

The goal of CADRE (CubeSat-investigating Atmospheric Density Response to Extreme driving) [2,47] is to study thermosphere properties. The secondary payload on CADRE is a dual frequency GPS receiver. The receiver will measure phase delays between two transmissions from the GPS constellation, L1 (1575.42 MHz) and L2 (1227.6 MHz). At transmission, L1 and L2 are in phase; the atmospheric media through which the signals pass introduces phase delays between the two signals. A measurement of the delay is used to measure TEC (Total Electron Content) of the ionosphere and density measurements of the troposphere.

1.7.3 ^{3}CAT 2

^{3}Cat 2 [5,48] is a 6U CubeSat developed at the Universidad Politécnica de Cataluña (UPC) to demonstrate a novel dual frequency (L1+L2) GNSS-R altimeter. The mission is designed to perform ocean altimetry by means of GNSS Reflectometry (GNSS-R). The main payload is the novel dual-band altimeter P(Y) & C/A ReflectOmeter (PYCARO), designed and manufactured at UPC Remote Sensing Lab and NanoSat Lab. Measuring GNSS signals reflected from the Earth allows performing simultaneous observations of the Earth on several points over a very wide swath, very promising for applications such as mesoscale altimetry.
It also integrates the Mirabilis Star Tracker, an experimental star tracker for attitude determination and the AMR eLISA magnetometer designed and manufactured at IEEC for the future ESA's LISA mission.

1.8 Micro-Bolometers

The bolometer is a device for measuring the power of incident electromagnetic radiation via the heating of a material with a temperature-dependent electrical resistance. Bolometers have flat spectral response, are very stable and robust to on-orbit degradation. Bolometers can be efficiently used on board small satellites for measurements of Solar Spectral Irradiance (SSI), a crucial measurement for climate modeling.

1.8.1 CSIM

CSIM– the Compact Solar Spectral Irradiance Monitor [49,50], developed by the LASP, University of Colorado and the Quantum Electronics and Photonics Division of the National Institute of Standards and Technology (NIST), Boulder, Colorado, represents a new generation of bolometric detectors based on a micro-machined silicon substrate with a silicon nitride thermal link and using multiwall vertically aligned carbon nanotubes (VACNTs) as black absorber.
The design provides a simple light path: entrance slit-prism-exit slit-detector, wavelength is scanned by rotating the prism; the electrical substitution radiometer provides long-term stability to calibrate the photodiodes and carries the absolute calibration. CSIM incorporates two identical channels, stacked on top of each other, to permit tracking of exposure-induced degradation.
The bolometer is implemented as a paired electrical substitution radiometer, thermistors on the two bolometers form one arm of a resistance bridge. A fixed heater power level is applied to the reference bolometer, the heater power applied to the active bolometer is adjusted to keep the bridge in balance (V_B=0). To measure optical power, the active bolometer is illuminated; the measured optical power is the change in heater power applied to the active bolometer. The design is based on vertically aligned carbon nanotubes (characterized by being extremely black, spectrally flat and with large thermal conductivity), a silicon substrate, a SiN thermal link (low thermal conductivity and mass), patterned heaters and leads, bonded thermistor.

These technologies both ease fabrication and provide higher performance: a continuous spectral irradiance in the 210-2400 nm, covering 96% of the total solar output, a noise level of 260 pW for a 40 s measurement.

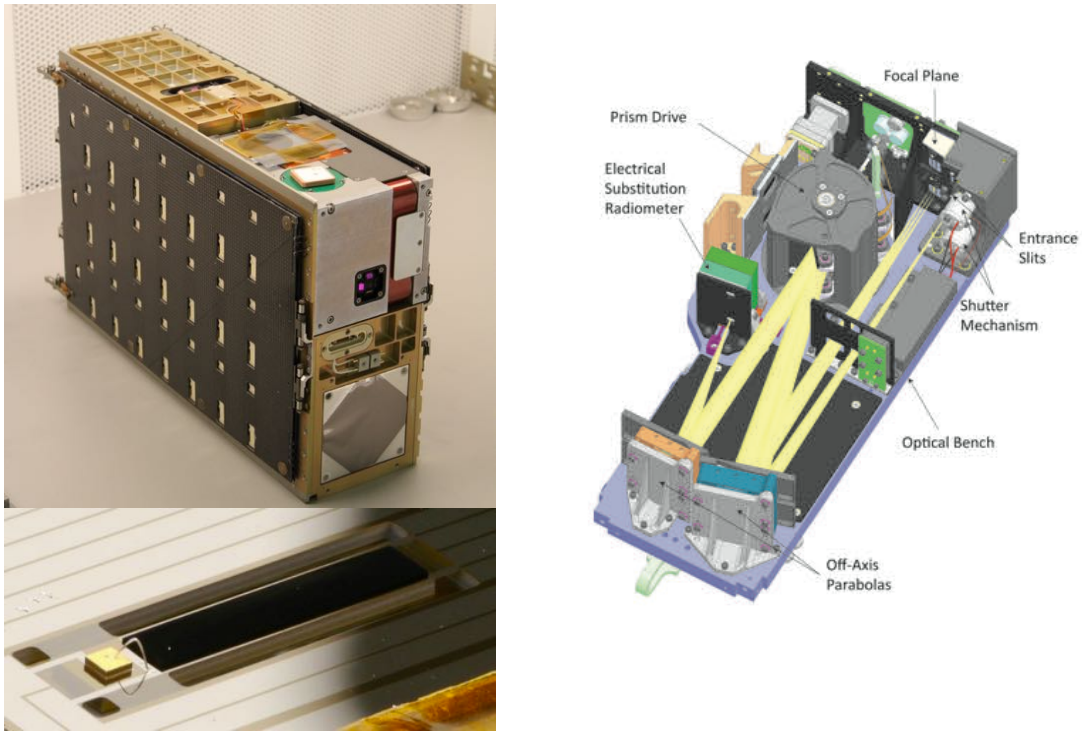

Figure Error! No text of specified style in document..**13**: Left: top - the CSIM prototype, bottom – the bolometer prototype. Right: optical overview [49,50] (image credit: LASP).

1.9 Radiometers

Three missions represent the status of the art of radiometers for small satellites and CubeSat in particular.

1.9.1 TEMPEST

The Temporal Experiment for Storms and Tropical Systems Demonstration (TEMPEST-D) [2,51,52] is a 6U CubeSat mission with a five-frequency millimeter-wave radiometer currently on orbit. The Earth Venture mission concept is to fly a constellation of identical TEMPEST CubeSats to observe the fine-scale temporal development of clouds and precipitation at 5-minute intervals.
Another example is the Radiometer Assessment using Vertically Aligned Nanotubes (RAVAN) 3U CubeSat that will demonstrate a payload that could be incorporated into a CubeSat or hosted payload constellation for measuring Earth radiation budget.
It is worth mentioning also the Time-Resolved Observations of Precipitation Structure and Storm Intensity with a Constellation of Smallsats (TROPICS) mission that will allow to make rapid revisits, allowing its microwave radiometers to measure temperature, humidity, precipitation, and cloud properties as frequently as every 21 minutes.

The TEMPEST radiometer, chosen as the reference radiometer here, performs continuous measurements at five frequencies, 89, 165, 176, 180 and 182 GHz. The instrument design is based on a 165 GHz to 182 GHz radiometer design inherited from RACE and an 89 GHz receiver developed under the ESTO ACT-08 and IIP-10 programs at CSU (Colorado State University) and JPL. The radiometer is based on the direct-detection architecture: the RF input to the feed horn is amplified, band-limited, and detected using Schottky diode detectors. The use of direct-detection receivers based on InP HEMT MMIC LNA front ends substantially reduces the mass, volume and power requirements of these radiometers. Input signals are band-limited using waveguide-based band-pass filters to meet the radiometer bandwidth requirements of 4±1 GHz at center frequencies of 89 and 165 GHz, as well as 2±0.5 GHz at 176, 180 and 182 GHz center frequencies [53].
The TEMPEST-D instrument occupies a volume of 3U and is mounted on a temperature-controlled bench that interfaces with the spacecraft structure using thermally isolating spacers.
The radiometer performs cross-track scanning, measuring the Earth scene between ±45° nadir angles, providing an 825 km wide swath from a 400 km nominal orbit altitude. Each radiometer pixel is sampled for 5 ms. The

radiometer performs end-to-end calibration during each rotation of the scanning reflector. The radiometer observes both cosmic background radiation at 2.7 K and an ambient blackbody calibration target (at approximately 300 K) every 2 seconds, for a scan rate of 30 rpm. A schematic representation of the TEMPEST-D observing profile over a 360° reflector scan and the resulting output data time series are shown in

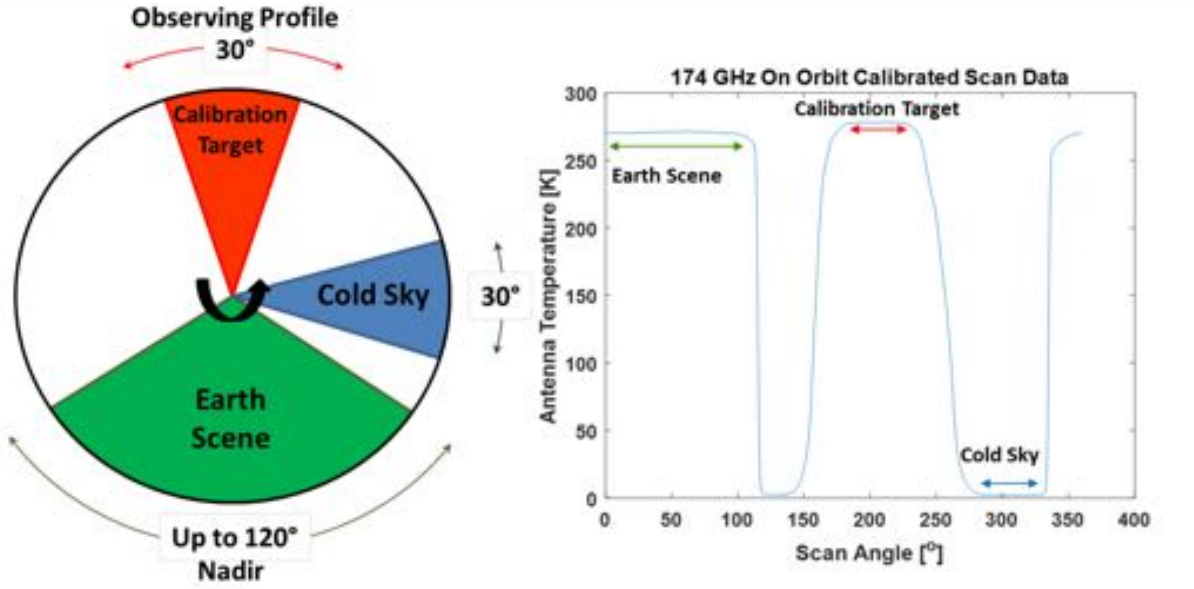

Figure Error! No text of specified style in document.**.14**: Schematic representation of TEMPEST-D observing profile (left) and output data time series (right) for each reflector scan (image credit: TEMPEST-D collaboration) [54]

1.10 Radar Systems

Radar systems are active systems that transmit a beam of radiation in the microwave region of the electromagnetic spectrum. Unlike optical systems that rely on reflected solar radiation or thermal radiation emitted by Earth, imaging radar instruments work independently of light and heat.

1.10.1RAX

The primary mission objective RAX and RAX-2 [2,55] is to study plasma instabilities that lead to magnetic field-aligned irregularities (FAI) of electron density in the lower polar thermosphere (80-300 km). These irregularities are known to disrupt communication and navigation signals. The RAX mission uses a network of existing ground radars that scatter signals off the FAI to be measured by a receiver on the RAX spacecraft (bistatic radar measurements) [5].

RAX mission measures the 3D k-spectrum (spatial Fourier transform) of ~1 m scale FAI as a function of altitude, with high angular resolution (~0.5º), in particular measuring the magnetic field alignment of the irregularities. The spacecraft will measure “radio aurora", the Bragg scattering from FAI that are illuminated with a narrow beam incoherent scatter radar (ISR) on the ground. The scattering locations are determined using a GPS-based synchronization between ISR transmissions and satellite receptions and the assumption that the scattering occurs only inside the narrow ISR beam.

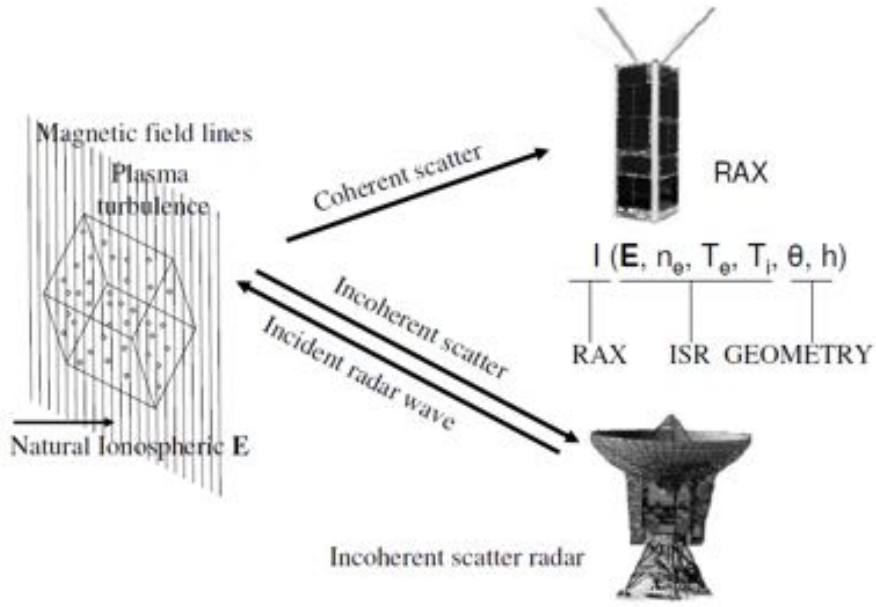

Figure **Error! No text of specified style in document.**.15 shows a drawing of the irregularities (red wiggles), the magnetic field lines, the radar beam, radio aurora (cones) and the satellite (cubes), and the satellite tracks. The irregularities inside the narrow radar beam and at a given altitude scatter the signals in a hollow cone shape. The thickness of the wall of each cone is a measure of magnetic aspect sensitivity, which is also a measure of plasma wave energy distribution in the parallel and perpendicular directions with respect to the geomagnetic field.

The radar receiver is capable of operation with five UHF ISRs (Incoherent Scatter Radars): PFISR (Poker Flat Incoherent Scatter Radar), Poker Flat, AK; RISR (Resolute Bay Incoherent Scatter Radar), Alberta, Canada; ESR (EISCAT Svalbard Radar, in Longyearbyen, Spitzbergen, Norway); Millstone Hill ISR of MIT in Westford, MA, USA, and Arecibo ISR in Puerto Rico. The ground-based ISR emits high-power radio frequency (RF) pulses into the ionosphere to be scattered off the FAI structures. Alternative ground radars are also being examined to achieve a greater number of experiments. The RAX payload receiver, developed at SRI, operates in a snapshot acquisition mode collecting raw samples at 1 MHz for 300 s over the experimental zone. Following each experiment, the raw data is post-processed for range-time-intensity and Doppler spectrum. The snapshot raw data acquisition enables flexibility in forming different radar pulse shapes and patterns. In addition, the PFISR electronic beam steering capability can be utilized for simultaneous multiple beam position experiments. The receiver can also operate with the MUIR radar located at the HAARP (High Frequency Active Auroral Research Program) facility in Gakona, AK, as part of active experiments.

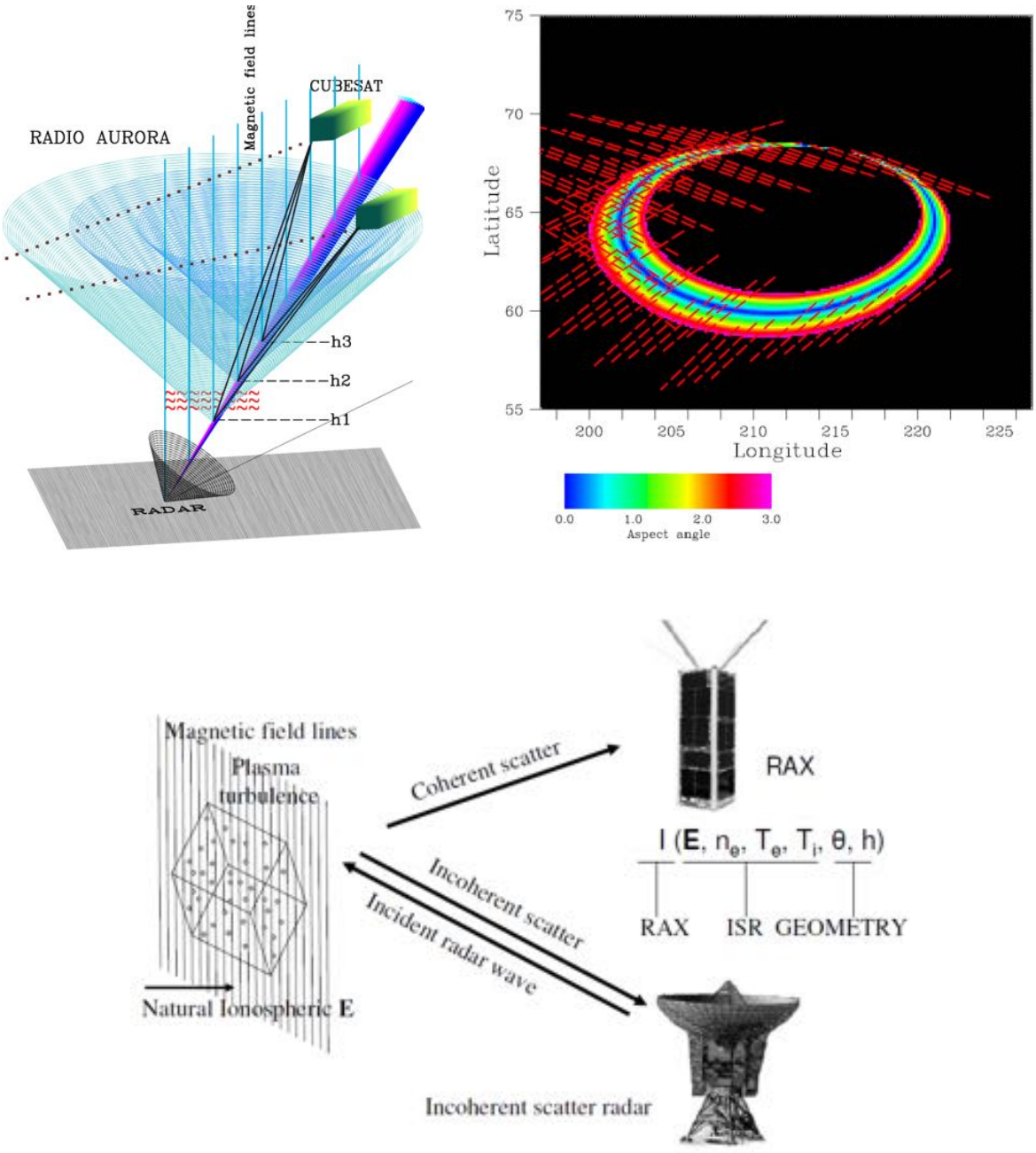

Figure Error! No text of specified style in document.**.15** Top Left and bottom: an illustration of the RAX experiment measurement concept. Top Right: the loci of perpendicularity (< 3º) and 1 min satellite tracks over the experimental zone over 30 days. (Reproduced/Adapted with permission from Hasan Bahcivan, SRI International, Menlo Park, CA, USA)

1.10.2 Radar Altimeters and SAR (EO)

Radar altimeters [56] are active sensors that use the ranging capability of radar to measure the surface topography profile along the satellite track. They provide precise measurements of a satellite height above the ocean by measuring the time interval between the transmission and reception of very short electromagnetic pulses. Altimetry satellites provide important ocean surface topography, currents, and surface winds that are essential for all shipping services (scientific and commercial). The information generated by ocean sensing radars is crucial for weather predictions and global weather models. The working principle of a radar altimeter is given in Figure Error! No text of specified style in document.**.16**.

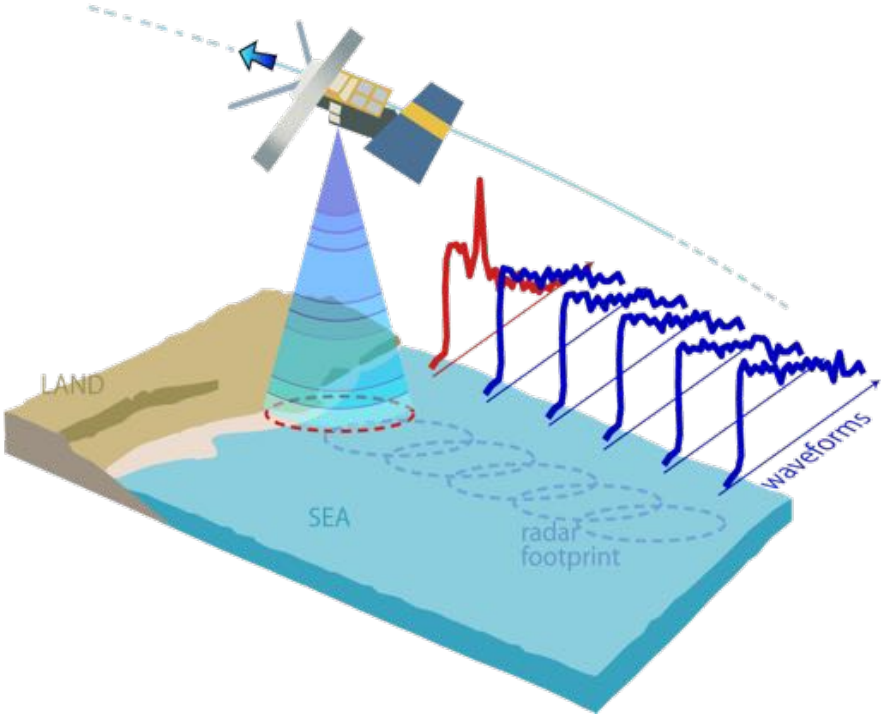

Figure Error! No text of specified style in document..**16**: Working principle of radar altimetry: Altimeter received waveforms in sea to land transition illustration (COASTALT portal and http://www.altimetry.info/)

Synthetic Aperture Radar (SAR) [57] can provide day-and-night imagery of Earth. Being a radar system, clouds, fog and precipitation do not have any significant effect, so that images can also be acquired independent of weather conditions. SAR profits of the motion of the radar antenna, mounted on board a satellite, above a target region to provide high spatial resolution images; its working principle is schematically shown in Figure Error! No text of specified style in document..**17**.

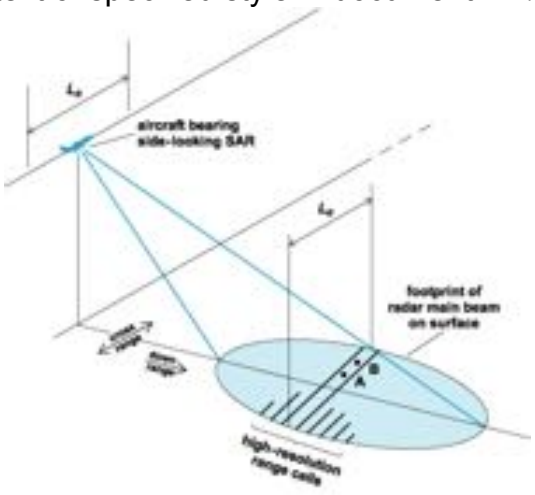

Image Credit: McGraw-Hill

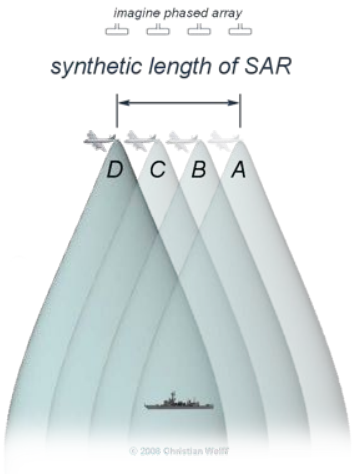

Image Credit: Christian Wolff

Figure Error! No text of specified style in document..**17**: Schematic working principle of a SAR: range resolution achieved through pulse compression of broad-bandwidth pulse; cross-range resolution achieved with Doppler processing. Photo: ESA - https://www.esa.int/OurActivities/ObservingtheEarth/Copernicus/SARmissions

For small satellites, SAR applications are physically limited by a number of factors [58]: the size (3U), the power/thermal capacity preventing the global coverage, a low orbit and no station keeping implying additional absolute height errors, using a Ku transmitter-receiver In order to meet these requirements, the working principle of radar altimetry as the one implemented in Topex/Poseidon has been reduced: typically a single frequency is used and a ionosphere model is implemented, a single pulse (SNR of ~ 7 dB is achievable), no radiometer and implementing a troposphere model, no DORIS and use GPS and retro-reflectors to derive the satellite velocity.

Many science applications require sub-cm level deformation measurements, but each individual SAR measurement is corrupted by up to several cm of atmospheric noise. Multiple acquisitions need to be averaged together to reduce atmospheric artifacts.

1.10.3 SRI-CIRES

SRI International [59] has designed and developed a miniaturized SAR payload for CubeSats at 500 km altitudes. SRI leverages expertise in airborne SAR and interferometric-synthetic aperture radar (InSAR) to create an S-Band radar subsystem capable of InSAR operations for the CubeSat platform. The radar subsystem has a volume less than 1.5 U (10Å~10Å~15 cm), mass of 1.5 kg, and low phase noise (e.g., accurate, stable reference clock). The goal is to achieve 20-meter spatial resolution and high-quality imaging (SNR>13dB) using a 5 m^2 supporting antenna and to obtain sub-centimeter level ground deformation accuracy. The payload subsystem is made of three modules: Power Amplifier (PA), Transmit/ Receive (TX/RX), and High Speed TX/RX Processor for real-time processing and storage of raw I/Q data and on-board processing of stored data.

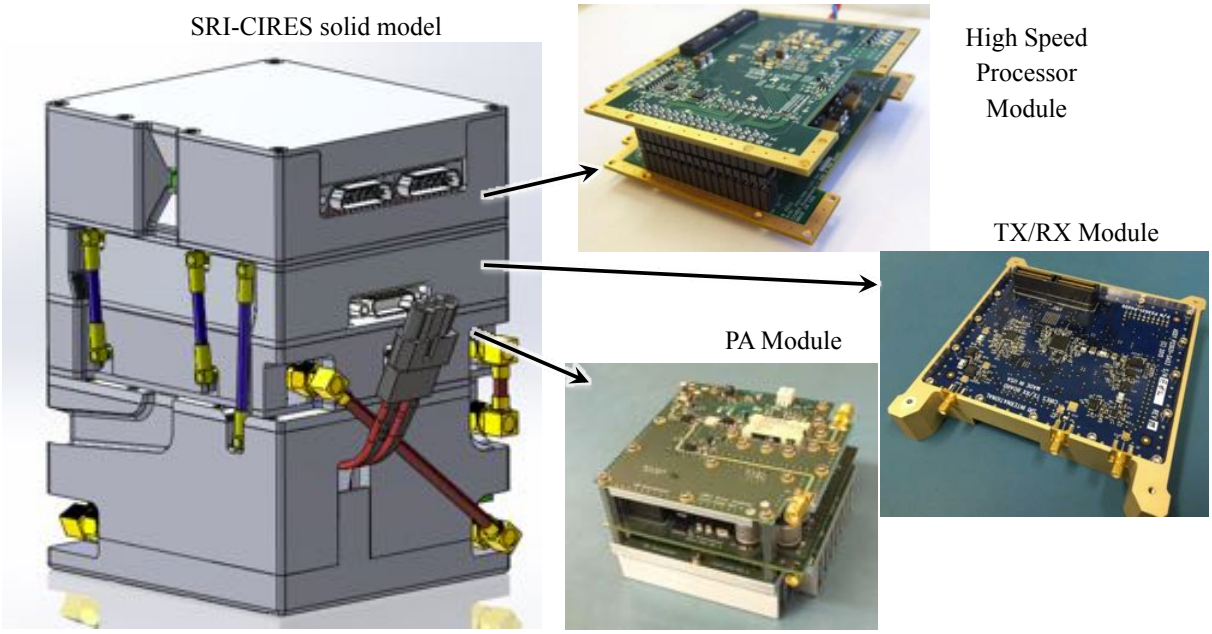

Figure Error! No text of specified style in document..**18**: SRI-CIRES illustration (Credit: SRI International)

1.11 Particle Detectors

Particle detectors is a wide range category of detectors, spanning from detectors measuring trapped electrons and protons, solar particles or even cosmic rays. In the following sections the most representative experiments are summarized.

1.11.1 REPTILE

REPTile [60] is a small (6.05 cm in length and 6 cm in diameter), low-mass, and low-power article detector on board CSSWE (Colorado Student Space Weather Experiment) capable of measuring relativistic outer radiation belt electrons in the energy range from 0.5 to 3 MeV and solar energetic protons from 10-40 MeV [5]. The instrument is a scaled down version of the instrument built at LAST (Laboratory for Atmospheric and Space Physics) for NASA's RBSP (Radiation Belts Storm Probes) mission.

The REPTile instrument measures the outer belt electrons, both trapped and precipitating to study how the low rate and energy spectrum of the Earth outer radiation belt electrons evolves in four energy bands (0.5-1.5, 1.5-2.2, 2.2-2.9, and >2.9 MeV) and monitors the SEP protons associated with solar flares to study how flare location, magnitude, and frequency relate to the timing, duration, and energy spectrum of SEP protons that reach Earth in four energy channels (8.5-18.5, 18.5-25, 25-30.5, and 30.5-40 MeV).

The instrument is a loaded-disc collimated telescope; it consists of a stack of four solid-state doped silicon detectors (by Micron Semiconductor). The front detector has a diameter of 20 mm, while the following three are 40 mm across. The stack is contained in a tungsten chamber, encased in an aluminum outer shield. The materials choice is optimized for their ability to shield energetic particles and minimize secondary electron generation within the housing. Tantalum, a good compromise between stopping power and relatively low secondary particle generation, is used for the baffles within the collimator prevent electrons from scattering into the detector stack from outside the instrument 52º FOV and give the instrument a geometric factor of 0.52 sr cm^2.

Particles impinge on the detector stack producing electron-hole pairs in the doped semi-conductor; higher energy particles penetrate deeper into the stack. A bias voltage is applied to each detector to accelerate generated electrons to an anode where they are collected. Using coincidence logic, the electronics can determine the energy range of the particle. The total instrument mass is 1.25 kg, with a cylindrical envelope of 4.6 m (diameter) × 6.0 cm (length).

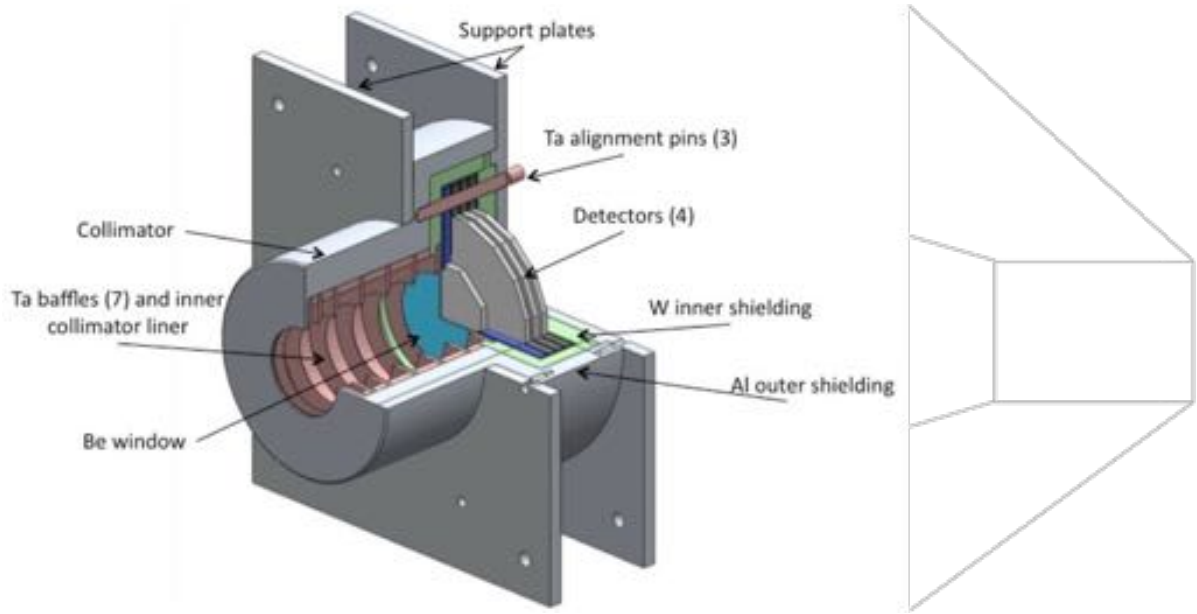

Figure Error! No text of specified style in document..**19**: Cutaway view of the REPTile instrument [61] (image credit: CU-Boulder)

1.11.2 EPISEM

The Edison Demonstration of SmallSat Networks (EDSN) mission [2,62,63] wants to demonstrate the feasibility of multi-point space weather observations with a swarm of eight identical satellites. EDSN, equipped with EPISEM (Energetic Particle Integrating Space Environment Monitor) to simultaneously monitor spatial and temporal variations in penetrating radiation above the atmosphere is important for understanding both the near-Earth radiation environment and as input for developing more accurate space weather models.

The EPISEM card [64] consists of a Geiger-Mueller tube mounted on a PCB and is designed to consume approximately 100 mW during operation. The GPS card enables time- and location-correlation of the EPISEM science data. By combining data and position/time information, it is possible to characterize the variability of penetrating high-energy protons at a much smaller scale than previously accomplished. EPISEM employs a thin-walled Geiger-Mueller tube located inside the spacecraft structure that detects penetrating beta/gamma radiation from energetic particles above a certain energy threshold, the threshold being different for electrons and protons. Incoming radiation knocks electron off of the Neon fill gas, Neon becomes Ne+ and free electron avalanches toward anode.

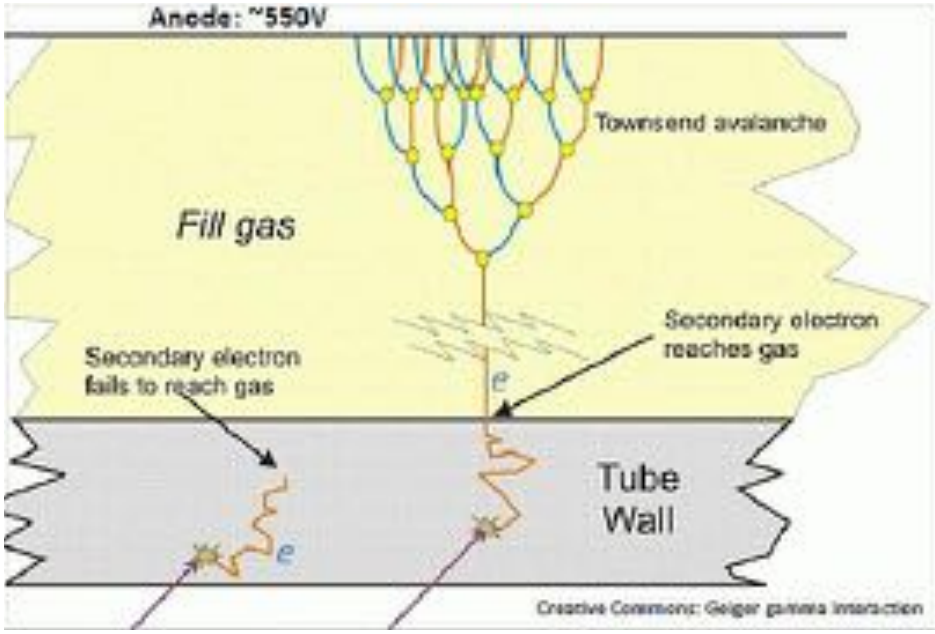

Figure Error! No text of specified style in document..**20**: Schematic view of interactions in the Geiger-Mueller tube of the EPISEM (image credit: NASA & MSU)

1.11.3 FIRE

The FIREBIRD mission [2,65,66] goal is to study the spatial scale and spatial temporal ambiguity of magnetosphere microbursts in the Van Allen radiation belts, and to provide spectral properties at medium energies. The mission concept is made of two spacecrafts. Each satellite carries two solid-state detector charged particle sensors with different geometric factors optimized to cover electron measurements over the energy range from 0.25 to ~1 MeV in six differential energy channels.

FIRE (Focused Investigations of Relativistic Electrons), developed by UNH, employs a heritage sensor design based on a single large-geometry-factor, solid-state detector set on each of the two spacecrafts, sensitive to electrons precipitating from the radiation belts. The detectors are read out by a Dual Amplifier Pulse Peak Energy Rundown, a customized ASIC (Application-Specific Integrated Circuit) by The Aerospace Corporation. Fast sample observations are stored by the on-board memory; survey observations identify times of interest to retrieve the highest temporal resolution data.

1.12 Plasma Waves Analysers

Plasma Wave Analysers measure the electric and magnetic fields and electron density and temperature in the interplanetary medium and planetary magnetospheres usually thanks to the use of Langmuir probes. Indeed, one of the most fundamental parameters to observe the space environment is the electric field that drives the motion of the plasma in the Earth ionosphere and magnetosphere.
In this category also magnetometer sensors are included, encompassing several types of detectors for magnetic field variations, such as Fluxgate magnetometers, search-coil magnetometers, which detects variations of the magnetosphere of very large-scale objects (planets, moons, or the Sun).

1.12.1 CADRE / WINCS

The overall objective of CADRE (CubeSat-investigating Atmospheric Density Response to Extreme driving) [2,67] is the study of thermosphere properties. Earth ionosphere and thermosphere are driven in a variety of regions on multiple scales; changes in the upper atmosphere can affect our society with its increasingly usage of space-based infrastructure.

WINCS (Wind Ion Neutral Composition Suite) is the primary payload of the CADRE mission, developed by NASA/GSFC and the Naval Research Laboratory (NRL). The size is 7.6 cm × 7.6 cm × 7.1 cm with a mass of ~ 0.850 kg, the power consumption is 1.3 W. The WINCS is made of four instruments [67], see also Figure Error! No text of specified style in document..**21**:

• WTS (Wind and Temperature Spectrometer)
• IDS (Ion Drift and temperature Spectrometer)
• NMS (Neutral Mass Spectrometer)
• IMS (Ion Mass Spectrometer).

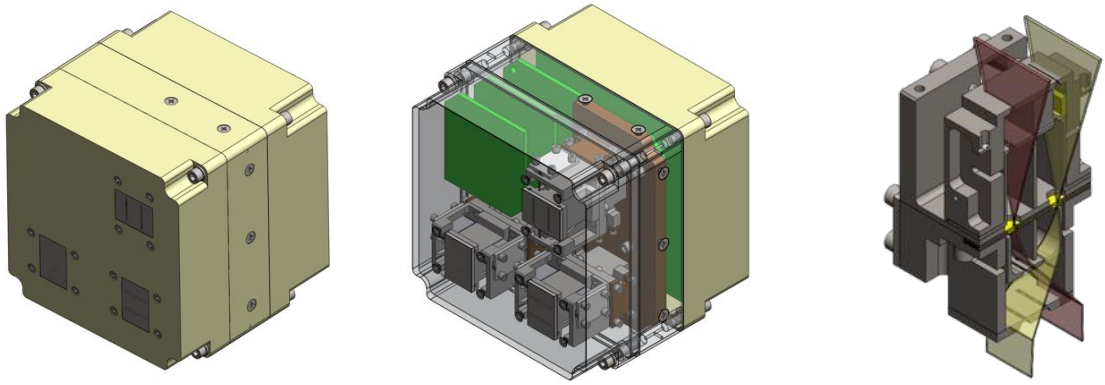

Figure Error! No text of specified style in document..**21**: Illustration of the WINCS package with individual instrument apertures (image credit: NASA, NRL) Left: layout of the 4 WINCS spectrometers: WTS and IDS consists of two spectrometer modules with mutually perpendicular FOVs as shown by the two pairs of long slits on the right side of the figure. The two round apertures on the other module show the parallel ion and neutral paths through the instrument. The multi-chamber WTS/IDS pair provides four separate chambers for photon rejection.

SDEA (Small-Deflection Energy Analyzer) is the core instrument of WTS/IDS. Ions enter the SDEA horizontally and deflect as they continue toward the exit slit; the exit slit plane is a circular cylinder section with vertical axis passing through the entrance slit - this defines the angle imaging function of SDEA. The upper and exit plates are biased at voltage V_{SDEA} (< 10 V) while the entrance and lower plates are at ground potential. The inhomogeneous field produced in the upper left region of the cavity produces the focusing in the incident ions, this reduces the size of exit slit and helps reducing unwanted UV photons that may reach the MCP (Micro Channel Plate) detector placed beyond the exit slit. The SDEA instrument has two identical mirrored sensors; one half of the SDEA is used for ions while the other half for neutrals.
The measurements are obtained from the angular and energy distributions of the particle flux. Two separate and orthogonal analyzers (WTS1 and WTS2 in Figure Error! No text of specified style in document..**21**) measure the angular energy distributions, both pointing within a few degrees of the ram direction. Each analyzer spans 30º × 2º FOV in 15 pixels, each 2º × 2º pixel scanning in 20 energy steps with the energy analyzer voltage to determine particle velocity. The position of maximum flux in each analyzer determines the horizontal and vertical angles in which the particles enter the detector.

The IMS/NMS (Ion Mass Spectrometer/Neutral Mass Spectrometer) uses two GEMS (Gated Electrostatic Mass Spectrometer) time-of-flight mass spectrometers developed at GSFC. GEMS uses a SDEA, turning the potential on and off. When the potential is off, particles impinging on the detector at the entrance slit continue straight forward along the SDEA and do not reach the exit slit; once the potential is turned on, charged particles are accelerated and deflected. The acceleration is a function of particle mass, their initial velocity being the same (orbital velocity): short after the potential turn on, low mass particles exit the slit (hydrogen needs to reach a kinetic energy of about 0.3 eV), followed after a while by heavier particles (iron needs a kinetic energy of about 18 eV). The final mass resolution $\Delta m/m$ is equal to the energy resolution $\Delta E/E$. The working principle is the same for IMS and NMS, so that the same potential levels; in both cases the acceleration is achieved by two-aperture ion optic lenses mounted above the respective entrance apertures of the GEMS. In the NMS ionization is produced by electron impact in its ion source.

1.12.2 DICE

DICE goal [2,68] is to map the geomagnetic SED (Storm Enhanced Density) plasma bulge and plume formations in Earth ionosphere. This objective is achieved via in-situ ionosphere measurements of electric field and plasma density. The measurements are made by two instruments; the EFP (Electric Field Probe) for electric field measurements and two separate two separate spherical fixed-bias DCP (DC Langmuir Probe) for absolute ion density measurements.

The EFP is based on the well-known electric field double-probe technique that monitors the potential of pairs of sensors, deployed on a boom several meters from the spacecraft, at a well-known distance. The electric field in the direction of the boom is measured by the ratio between the potential differences. The EFP is made of four sensors: a 1 cm diameter sphere, gold plated, mounted at the end of each of four wire booms. Each sensor is mounted in a corner mount, also gold plated, shown in Figure Error! No text of specified style in document.**.22** that has a semi-sphere that cups the electric field probe sensor.

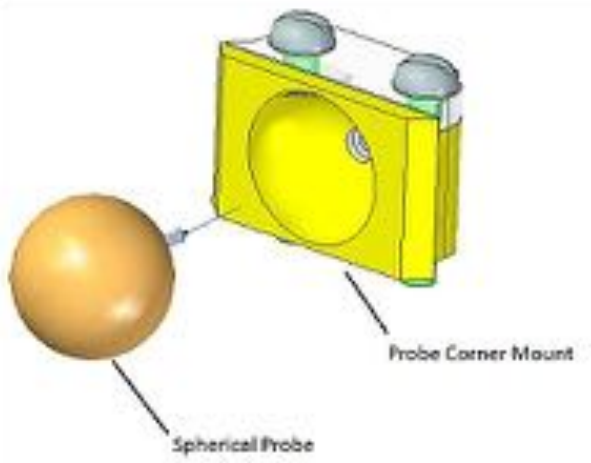

Figure Error! No text of specified style in document.**.22**: Corner mount geometry of the spherical probe (image credit: DICE consortium)

The EFP makes DC and AC electric field measurements, both at equal time steps. The DC measurements are made at an 8 Hz rate, providing 45º rotational resolution per spacecraft spin to maximize the science return; DC measurements are a subset of AC measurements performed at 4096 Hz.

The DCP sensors operate in the ion saturation region providing measurements of ion density in the range 2×10^9 to 2×10^{13} m^{-3} and a resolution of 3×10^8 m^{-3}. The two sensors are deployed on separate fiberglass cylindrical booms, 8 cm long, from the top and bottom of the spacecraft along its spin axis.

In addition to these two devices, a science-grade magnetometer, TAM (Three-Axis Magnetometer), is aimed at measuring field aligned currents. The TAM measurements allow accurate identification of storm-time features, with simultaneous co-located electric field measurements, previously missing, provided by EFP.

1.12.3 INSPIRE / CVHM

CVHM (Compact Vector-Helium Magnetometer) on board INSPIRE (Interplanetary NanoSpacecraft Pathfinder In a Relevant Environment) [2,69,70] is a JPL/UCLA instrument based on previous mission heritage (from Mariner, through Cassini missions), here significantly reducing the overall size: CVHM size are ~5 cm × 10 cm × 10 cm with a mass of 0.5 kg, still providing a very good stability, less than 10 pT, thus representing a significant improvement on previously flown CubeSat magnetometers.

The INSPIRE mission consists of two spacecrafts that separate after deployment. Spacecrafts make synchronous measurements of the solar-wind magnetic field as they slowly separate after launch for 90 days out to 1.5 million km from Earth. Depending upon trajectory (Earth-leading or Earth-trailing), the magnetometers may provide real-time measurements across the bow-shock of Earth magnetosphere, and a new look into turbulence effects.

1.13 Biological Detectors

A new discipline, called astrobiology, is recently entering the space field. As it is stated by EANA (European Astrobiology network Association) on http://eana-net.eu/index.php?page=Discover/esaexo, astrobiology is a life sciences activities that cover every aspect of space life sciences, including biology, physiology, biotechnology, biomedical applications, biological life-support systems, exobiology, animal research and access to ground facilities; thus a large amount of detectors can be included in this category. On small satellite side, here only one main mission is given: OREOS, since this represents the state of the art in this field.

1.13.1 OREOS

The overall objective of O/OREOS (Organism/ORganics Exposure to Orbital Stresses), [2,71,72,73] heritage of PharmaSat and GeneSat mission, is to test how life and the components of life respond to the radiation environment in space. The experiment carries up into space organisms and organic compounds and monitors the changes induced by the harsh radiation environment and microgravity. There are two on-board experiments, both including specimens: SESLO (Space Environment Survivability of Living Organisms) and SEVO (Space Environment Viability of Organics). Each of them is equipped with its own electronics, microcontroller, and data storage requiring only a standard power and-data interface.

The objective of the SESLO experiment is to characterize the growth, activity, health and ability of microorganisms to adapt to the stresses of the space environment. The experiment contains two types of living biological specimens, microbes, commonly found in salt ponds and soil, Halorubrum chaoviatoris and Bacillus subtilis; the experiment provides active optical measurement of growth and/or metabolic activity. SESLO is sealed in a vessel at one atmosphere, microbes are stored in a dried and dormant state.

Once OREOS is deployed in orbit, the experiment starts. It begins to rehydrate and grow three sets of the microbes at three different times, each test occurs in its own module, thermally isolated from the other two: 1. first test within 1-2 weeks after launch, 2. in the following three months, and 3. the final test at six months after launch. The payload uses time-resolved optical absorbance and density measurements to track the growth and metabolism of the organisms for both organisms, a technique inherited by the PharmaSat mission. A dedicated tricolor LED illuminates along the axis of each system and a detector at the opposite side reads the intensity for each color, with centre wavelengths at 470, 525, and 615 nm.

The objective of the SEVO experiment is to monitor the stability, modification, and degradation of organic molecules in specific space environments including interplanetary/interstellar space, the lunar surface, wet/salty environments, and the Martian atmosphere. SEVO consists of four experimental "micro-environments" containing miniature reaction cells of organic molecules, in thin-film form, representing chemical building blocks of life in our Solar System and beyond.

The chemical behavior of molecule exposure to solar UV and visible light, and space ionizing radiation is monitored by a spectrometer over the 6-month mission lifetime. The spectrometer profits of the heritage of previous NASA LCROSS (Lunar CRater Observation and Sensing Satellite) and LADEE (Lunar Atmosphere and Dust Environment Explorer) missions. The instrument covers the UV-Visible wavelength range (200 – 1000 nm) with a 1–2 nm spectral resolution and better than 0.1 nm spectral band-shift-measurement capability; it provides 0.03 absorbance-unit resolution. The detector acquires a single spectrum in less than 100 ms.

A pair of baffled diffuser assemblies ensure that the sample film is uniformly illuminated over a 3 mm diameter spot. Light intensity varies by less than ±25% for sun angles within ±35^{o} from normal, solar intensity sensors guarantee synchronous measurements for each spectral acquisition. The reaction cells are derived from those used for the EXPOSE experiment on the ISS. Each of the four organic materials is vacuum sublimed onto several MgF_2 windows, to allow UV-visible irradiation as short as 124 nm; some of the windows have either SiO_2 or Al_2O_3 thin coating layers between the organic and the MgF_2 to tune the band pass and provide a chemically substrate relevant to the corresponding micro-environment.

A sapphire window is chosen for its high optical transparency along the spectrometer wavelength band) and is placed on the far side, where light enters the collection optic and is routed to the spectrometer. Both windows are welded to a stainless-steel spacer providing a hermetically sealed micro-environment with the desired simulated atmosphere. The sealed cells are then assembled in 11 mm diameter housings and installed into the

rotatable payload carousel. The system is schematically shown in Figure Error! No text of specified style in document..**23**. This assembly also helps in protecting the fragile windows during the launch phase. Samples are staggered and divided into two concentric rings. Two optical fibers are placed under the carousel but, due to the cell spacing, only one fiber at a time is illuminated; their outputs are then combined for input to the spectrometer.

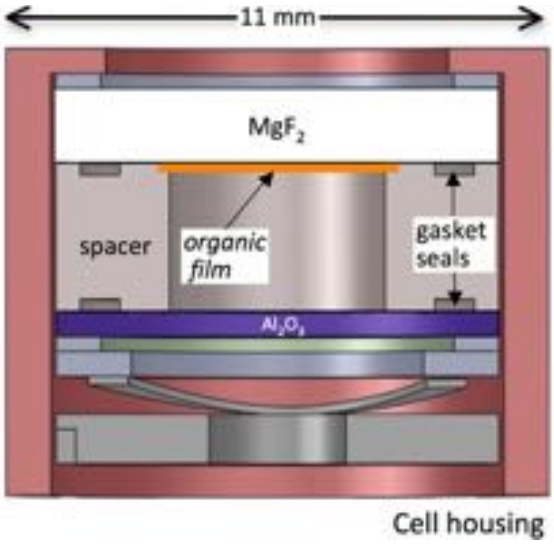

Figure Error! No text of specified style in document..**23**: Reaction cell cross section (image credit: NASA & Utah State University)

1.14 Solar Sails

Solar sails use sunlight to propel vehicles through space much like sailboats rely on wind to push through the water. NanoSail-D2 [2,74] depicted in Figure Error! No text of specified style in document..**24** (left) is a technology and science experiment designed to validate solar sail capabilities. NanoSail-D2 is a 10 square meter solar sail payload (Figure Error! No text of specified style in document..**24** - right) packaged within a 3U nanosatellite, designed and developed at NASA/MSFC (Marshall Space Flight Center) in partnership with NASA/ARC (Ames Research Center) and several industry and academic partners. The NanoSail D2 solar sail payload section occupies 2U or 2/3 volume of the spacecraft. Sail payload closeout panels provide protection for the sail and deployment booms during the launch phase of the mission, the panels have spring loaded hinges that were released on-orbit, using the auto timer command of the spacecraft bus.

One of NanoSail-D's several mission objectives is to demonstrate the capability to deploy a large sail structure from a highly compacted volume without re-contact with the spacecraft. This demonstration can be applied to deploy future communication antennas, sensor arrays or thin film solar arrays to power spacecraft. The mission also will demonstrate and test the de-orbiting capabilities of solar sails. NASA hopes to one day use thin membranes to de-orbit satellites and large space debris.

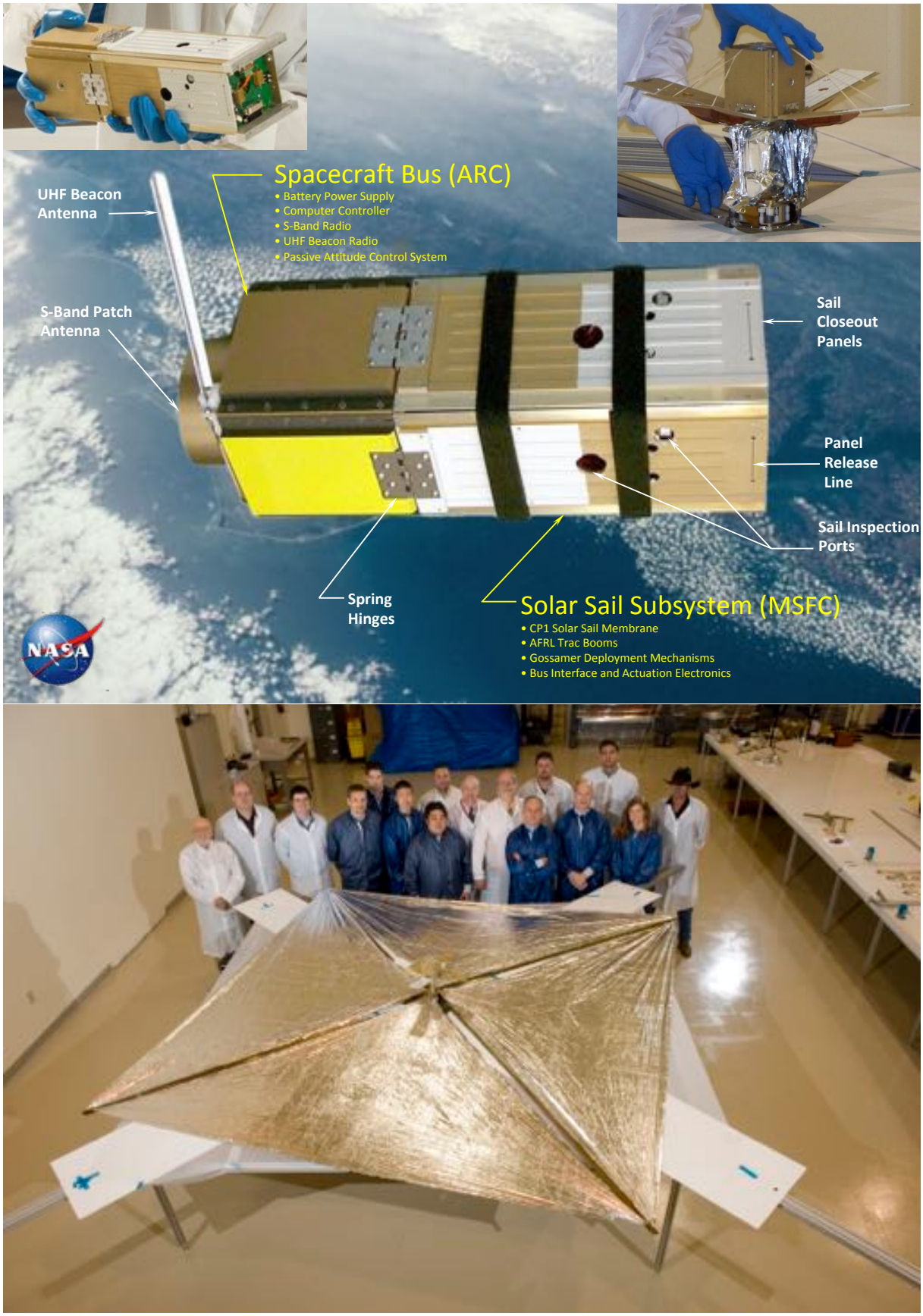

Figure Error! No text of specified style in document.**.24**: Top: on-orbit view of the NanoSail-D2 spacecraft before sail deployment (image credit: NASA/ARC). Bottom: Panel deployed configuration of NanoSail-D (image credit: NASA)

1.15 Conclusions

I hope that in these sections, it has been demonstrated that small satellites have great capabilities. I sincerely think that the potential of small satellites stays in the satellite system configuration meant as a swarm of satellites, located in different points in the near-Earth environment or even in the Solar system, that are working together to produce a combined result. This type of multi-point or constellation-type measurements provide much greater temporal coverage than that achievable with a single, large spacecraft.

Given this, at least a few more uses of small satellites shall be kept in mind. First CubeSats can prove the usage of a payload to demonstrate technology for future use on larger missions. CubeSats have indeed also additional advantages; they can provide observations that can mitigate the data gap between critical satellite systems in different scientific fields, e.g. Earth Observation or Space Weather to guarantee a prompt warning, because of their lower cost and shorter development time.

References

1. National Academies of Sciences, Engineering, and Medicine. 2016. Achieving Science with CubeSats: Thinking Inside the Box. Washington, DC: The National Academies Press. doi:10.17226/23503 NSF report
2. The EO Portal Satellite Missions Database https://directory.eoportal.org/web/eoportal/satellite-missions/
3. B. Lal, E. de la Rosa Blanco, J. R. Behrens, B. A. Corbin, E. K. Green, A. J. Picard, A. Balakrishnan, “Global Trends in Small Satellites”, Science & Technology Policy Institute, Institute for Defense Analyses - IDA Paper P-8638, July 2017
4. NATIONAL SCIENCE FOUNDATION (NSF), Cubesat-Based Science Missions For Geospace And Atmospheric Research, October 2013
5. Gunter's Space Page, URL: http://space.skyrocket.de/
6. Charles D. Norton, Steve A. Chien, Paula J. Pingree, David M. Rider, John Bellardo, James W. Cutler, Michael P. Pasciuto, “NASA’s Earth Science Technology Office CubeSats for Technology Maturation,” Proceedings of the 27th AIAA/USU Conference, Small Satellite Constellations, Logan, Utah, USA, Aug. 10-15, 2013, paper: SSC13-XI-4, URL of paper : http://digitalcommons.usu.edu/cgi/viewcontent.cgi?article=2987&context=smallsat
7. Paula J. Pingree, “Looking Up: The MCubed/COVE Mission,” Proceedings of the 11th Annual CubeSat Developers’ Workshop - The Edge of Exploration,” San Luis Obispo, CA, USA, April 23-25, 2014, URL: http://www.cubesat.org/images/.../DevelopersWorkshop2014/Pingree_MCubed_COVE_Mission.pdf
8. Dmitriy L. Bekker, Thomas A. Werne, Thor O. Wilson, Paula J. Pingree, Kiril Dontchev, Michael Heywood, Rafael Ramos, Brad Freyberg, Fernando Saca, Brian Gilchrist, Alec Gallimore, James Cutler, “A CubeSat Design to Validate the Virtex-5 FPGA for Spaceborne Image Processing,” Proceedings of the 2010 IEEE Aerospace Conference, Big Sky, MT, USA, March 6-13, 2010
9. Maurice Borgeaud, Noémy Scheidegger, Muriel Noca, Guillaume Roethlisberger, Fabien Jordan, Ted Choueiri, Nicolas Steiner, "SwissCube : The first entirely-built Swiss student satellite with an Earth observation payload," Proceedings of the 7th IAA Symposium on Small Satellites for Earth Observation, Berlin, Germany, May 4-7, 2009, IAA-B7-0205P, SwissCube URL: http://swisscube.epfl.ch/
10. Guillaume Roethlisberger, Fabien Jordan, Anthony Servonet, Maurice Borgeaud, Renato Krpoun, Herbert R. Shea, "Advanced Methods for Structural Machining and Solar Cell Bonding Allowing High System Integration and their Demonstration on a Pico-satellite," Proceedings of the 22nd Annual AIAA/USU Conference on Small Satellites, Logan, UT, USA, Aug. 11-14, 2008, SSC08-XI-4, URL: http://ctsgepc7.epfl.ch/12%20-%20SwissCube%20papers/G.Roethlisberger_SSC08-XI-4.pdf
11. Craig Underwood, Vaios J. Lappas, Chris Bridges, "AAReST Spacecraft DDR (Detailed Design Review): Spacecraft Bus, Propulsion, RDV/Docking and Precision ADCS," 2014, URL: http://pellegrino.caltech.edu/AAReST_Docs/AAReST_Surrey_DDR_2014.pdf

12. Sergio Pellegrino, "Autonomous assembly of a reconfigurable space telescope," URL: http://pellegrino.caltech.edu/aarest2.html
13. Keith Patterson, "Lightweight Deformable Mirrors for future Space Telescopes," Thesis In Partial Fulfillment of the Requirements for the Degree of Doctor of Philosophy," California Institute of Technology, Pasadena, CA, December 2013, URL: http://thesis.library.caltech.edu/8043/1/patterson_keith_2013_thesis.pdf
14. S. Palo, T. Woods, X. Li, J. Mason, M. Carton, A. Caspi, A. Jones, R. Kohnert, S. Solomon, "MinXSS: A Three-Axis Stabilized CubeSat for Conducting Solar Physics," 5th European CubeSat Symposium, Royal Military Academy, VKI (Von Karman Institute), Brussels, Belgium, June 3-5, 2013
15. Thomas N. Woods, Amir Caspi, Phil Chamberlin, Andrew Jones,Rich Konert, Xinli Li, Scott Palo, Stanley Solomon, "MinXSS - Miniature X-ray Solar Spectrometer (MinXSS) CubeSat Mission," Submitted to NASA on August 15, 2013, URL: http://www.pinheadinstitute.org/wp-content/uploads/2014/07/MinXSS_Proposal2013_NASA.pdf
16. P. Kaaret, K. Jahoda, B. Dingwall, "HaloSat – A CubeSat to Study the Hot Galactic Halo," URL: https://files.aas.org/head14/116-21Philip_Kaaret.pdf
17. Philip Kaaret, "HaloSat Overview," The University of Iowa, August 17, 2016, URL: http://astro.physics.uiowa.edu/~kaaret/2016f_a6880/halosat_overview.pdf
18. "Amptek Complete X-Ray Spectrometer," Amptek, URL: http://www.amptek.com/x123.html
19. Tyler G. Rose, Benjamin K. Malphrus, Kevin Z. Brown, “An Improved Measurement of the Diffuse X-Ray Background: The Cosmic X-Ray Background Nanosat (CXRN,” 8th Annual CubeSat Developers’ Workshop, CalPoly, San Luis Obispo, CA, USA, April 20-22, 2011, http://www.cubesat.org/images/2011_Spring_Workshop/thur_a9.30_rose_cxbn_cswkshp_sp2011.pdf
20. Kevin Z. Brown, Tyler G. Rose, Benjamin K. Malphrus, Jeffrey A. Kruth, Eric T. Thomas, Michael S. Combs, Roger McNeil, Robert T. Kroll, Benjamin J. Cahall, Tyler T. Burba, Brandon L. Molton, Margaret M. Powell, Jonathan F. Fitzpatrick, Daniel C. Graves, J. Garrett Jernigan, Lance Simms, John P. Doty, Matthew Wampler-Doty, Steve Anderson, Lynn R. Cominsky, Kamal S. Prasad, Stephen D. Gaalema, Shunming Sun, “The Cosmic X-Ray Background NanoSat (CXBN): Measuring the Cosmic X-Ray Background Using the CubeSat Form Factor,” Proceedings of the 26th Annual AIAA/USU Conference on Small Satellites, Logan, Utah, USA, August 13-16, 2012, paper: SSC12-VII-6
21. D. Casadei, N. Jeffrey and E.P. Kontar, “Measuring X-ray anisotropy in solar flares. Prospective stereoscopic capabilities of STIX and MiSolFA”, A&A 606 (2017) A2, doi:10.1051/0004-6361/201730629, MiSolFA URL https://misolfa.i4ds.net/mission/
22. G. Rottman, V. George, "An Overview of the Solar Radiation and Climate Experiment," The Earth Observer, May/June 2002, Vol. 14, No 3, pp. 17-22; Rottman, Woods, and Sparn (1993) Solar-Stellar Irradiance Comparison Experiment I. 1. Instrument Design and Operation, JGR, vol 98, D6, 10,667-10,677, doi:10.1029/93JD00462
23. SORCE URLs: http://lasp.colorado.edu/sorce/, http://earthobservatory.nasa.gov/Library/SORCE/, http://lasp.colorado.edu/home/sorce/mission/
24. “National Scientific Foundation (NSF) CubeSat-based science missions for Geospace and Atmospheric Research,” Annual Report, October 2013, pp: 36-37, URL: http://www.nsf.gov/geo/ags/uars/cubesat/nsf-nasa-annual-report-cubesat-2013.pdf
25. “OPAL (Oxygen Photometry of the Atmospheric Limb)”, USU/SDL, URL: http://www.sdl.usu.edu/downloads/opal.pdf
26. Alan Marchant, Mike Taylor, Charles Swenson, Ludger Scherlies, “Hyperspectral Limb Scanner for the OPAL Mission,” Proceedings of the AIAA/USU Conference on Small Satellites, Logan, Utah, USA, August 2-7, 2014, paper: SSC14-VII-5
27. "Lunar IceCube to Take on Big Mission From Small Package," NASA, August 4, 2015 (updated on Jan. 29, 2016), URL: https://www.nasa.gov/feature/goddard/lunar-icecube-to-take-on-big-mission-from-small-package
28. P. E. Clark, Ben Malphrus, Kevin Brown, Dennis Reuter, Robert MacDowall, David Folta, Avi Mandell, Terry Hurford, Cliff Brambora, Deepak Patel, Stuart Banks, William Farrell, Noah Petro, Michael Tsay, V. Hruby, Carl Brandon, Peter Chapin, "Lunar Ice Cube Mission: Determining Lunar

Water Dynamics with a First Generation Deep Space CubeSat," 47th Lunar and Planetary Science Conference (2016), The Woodlands, Texas, March 21-25, 2016, paper: 1043.pdf, URL: http://www.hou.usra.edu/meetings/lpsc2016/pdf/1043.pdf

29. Charles D. Norton, Michael P. Pasciuto, Paula Pingree, Steve Chien, David Rider, "Spaceborne Flight Validation of NASA ESTO Technologies," Proceedings of IGARSS (International Geoscience and Remote Sensing Symposium), Munich, Germany, July 22-27, 2012, URL: http://tinyurl.com/qgbzr9b
30. GRIFEX URL: http://cubesat.jpl.nasa.gov/projects/grifex/overview.html
31. Panchromatic Fourier Transform Spectrometer (PanFTS). 2nd GEO-CAPE Community WorkshopMay 12, 2011
32. S. Sander, D. Bekker, J-F. Blavier, M. Bryk, C. Donahue, R. Goullioud, B. Hancock, D. Johnson, R. Key, A. Lamborn, K. Manatt, J. Moore, J. Nastal, T. Neville, D. Preston, D. Rider, M. Ryan, J. Wincentsen, and Y.-H. Wu "Panchromatic Fourier Transform Spectrometer Engineering Model (PanFTS-EM) for Geostationary Atmospheric Measurements", Fourier Transform Spectroscopy 2015, Lake Arrowhead, California United States, 1–4 March 2015. ISBN: 978-1-55752-814-8 .
33. "HyperCubeTM3D Wind Measurement," Harris Corporation, 2017, URL: https://www.harris.com/sites/default/files/downloads/solutions/55493_hypercube_data-sheet_v2_2_final_.pdf
34. Ronald Glumb, Michael Lapsley, Peter Mantica, Anna Glumb, "TRL6 Testing of Hyperspectral Fourier Transform Spectrometer Instrument for CubeSat Applications," Proceedings of the 31st Annual AIAA/USU Conference on Small Satellites, Logan UT, USA, Aug. 5-10, 2017, paper: SSC17-VI-08,URL: http://digitalcommons.usu.edu/cgi/viewcontent.cgi?article=3641&context=smallsat
35. T. N. Woods, G. Rottman, R. Vest, "XUV Photometer System (XPS): Overview and Calibration," Solar Physics, Vol. 230, No 1-2 (Special issue of SORCE), Aug. 2005, pp. 345-374
36. XPS URL: http://lasp.colorado.edu/sorce/instruments/xps/xps_instrument_design.htm
37. N. C. Deschamps, C. C. Grant, D. G. Foisy, R. E. Zee, A. F. J. Moffat, W. W. Weiss, "The BRITE Space Telescope: A Nanosatellite Constellation for High-Precision Photometry of Bright Stars," Proceedings of the 20th Annual AIAA/USU Conference on Small Satellites, Logan, UT, Aug. 14-17, 2006, paper: SSC06-X-1, URL: http://www.utias-sfl.net/docs/brite-ssc-2006.pdf
38. N. C. Deschamps, C. C. Grant, D. G. Foisy, R. E. Zee, A. F. J. Moffat, W. W. Weiss, "The BRITE Space Telescope: Using a Nanosatellite Constellation to Measure Stellar Variability in the Most Luminous Stars,," Proceedings of the 57th IAC/IAF/IAA (International Astronautical Congress), Valencia, Spain, Oct. 2-6, 2006, IAC-06-B5.2.7, URL: http://www.utias-sfl.net/docs/brite-iac-2006.pdf;
39. Arcsecond Space Telescope Enabling Research in Astrophysics (ASTERIA), NASA/JPL, URL: http://www.jpl.nasa.gov/cubesat/missions/asteria.php
40. Matthew W. Smith, Sara Seager, Christopher M. Pong, SungyungLim, Matthew W. Knutson, Timothy C. Henderson, Joel N. Villaseñor, Nicholas K. Borer, David W. Miller, Shawn Murphy, "ExoplanetSat:A Nanosatellite Space Telescope for Detecting Transiting Exoplanets," 8th Annual CubeSat Developers' Workshop, CalPoly, San Luis Obispo, CA, USA, April 20-22, 2011
41. Matthew W. Smith, Sara Seager, Christopher M. Pong, Jesus S. Villaseñor, George R. Ricker, David W. Miller, Mary E. Knapp, Grant T. Farmer, Rebecca Jensen-Clem, "ExoplanetSat: Detecting transiting exoplanets using a low-cost CubeSat platform," Proceedings of SPIE, 'Space Telescopes and Instrumentation 2010: Optical, Infrared, and Millimeter Wave,' edited by Jacobus M. Oschmann, Mark C. Clampin, Howard A. MacEwen, SPIE, Vol. 7731, San Diego, CA, USA, June 2010, doi:10.1117/12.856559, URL: http://dspace.mit.edu/openaccess-disseminate/1721.1/61644
42. Christopher M. Pong and Matthew W. Smith, "Camera modeling, centroiding performance, and geometric camera calibration on ASTERIA," 2019 IEEE Aerospace Conference, Big Sky, MT, 2019, pp. 1-16.
43. Ref. E. Hand, 2012, Microsatellites aim to fill weather-data gap, Nature 491(7426):650-651
44. Christopher Ruf, "The NASA EV-2 Cyclone Global Navigation Satellite System (CYGNSS) Mission ," August 27, 2012, URL of presentation: http://svcp.jpl.nasa.gov/meetings/2012/es/082701/CYGNSS_27Aug2012_Ruf_CYGNSS_JPL_Seminar.pdf

45. Christopher S. Ruf, Scott Gleason, Zorana Jelenak, Stephen Katzberg, Aaron Ridley, Randall Rose, John Scherrer, Valery Zavorotny, "The CYGNSS Nanosatellite Constellation Hurricane Mission," Proceedings of IGARSS (International Geoscience and Remote Sensing Symposium), Munich, Germany, July 22-27, 2012
46. http://www.sstl.co.uk/getattachment/8ea1074b-b37a-4829-8345-b1bb02656d02/SGR-ReSI, http://ktb.engin.umich.edu/RSG/pubsfiles/AeroConf-2013Unwin-etalSGR-ReSI.pdf
47. James W. Cutler, Aaron Ridley, Andrew Nicholas, "CubeSat Investigating Atmospheric Density Response to Extreme Driving (CADRE)," Proceedings of the 25th Annual AIAA/USU Conference on Small Satellites, Logan, UT, USA, Aug. 8-11, 2011, paper: SSC11-IV-7, URL: http://rax.engin.umich.edu/wp-content/uploads/files/CADRE-SmallSat-2011.pdf
48. 3Cat 2 URL: https://nanosatlab.upc.edu/en/missions-and-projects/3cat-2
49. A Compact Solar Spectral Irradiance Monitor for Future Small Satellite and CubeSat Science Opportunities, Challenges & Opportunities in Solar Observations, 12 Nov. 2015
50. New Generation Bolometric Detector for Measurement of Solar Spectral Irradiance, Jan 2017 AMS American Meteorological Society
51. Anne Ju Manning, "Small satellites to pave way for future space-borne weather observations," CSU, Dec. 2015, URL: http://source.colostate.edu/small-satellites-to-pave-the-way-for-future-space-borne-weather-observations/
52. Reising, S. C., T. C. Gaier, S. Padmanabhan, B. H. Lim, C. D. Kummerow, V. Chandrasekar, W. Berg, C. Heneghan, R. Schulte, C. Radhakrishnan, S. T. Brown, and M. Pallas, “Temporal Experiment for Storms and Tropical Systems Technology Demonstration (TEMPEST-D) to Enable Temporally-Resolved Observations of Clouds and Precipitation on a Global Basis Using 6U-Class Satellite Constellations,” In: Proc. NASA Earth Science Technology Forum (ESTF 2018), Silver Spring, Maryland, June 2018, A3P6.
53. Steven C. Reising, Christian D. Kummerow, V. Chandrasekar, Wesley Berg, Jonathan P. Olson, Todd C. Gaier, Sharmila Padmanabhan, Boon H. Lim, Cate Heneghan, Shannon T. Brown, John Carvo, Matthew Pallas, "Temporal Experiment for Storms and Tropical Systems Technology Demonstration (TEMPEST-D) Mission: Enabling Time-Resolved Cloud and Precipitation Observations from 6U-Class Satellite Constellations," Proceedings of the 31st Annual AIAA/USU Conference on Small Satellites, Logan UT, USA, Aug. 5-10, 2017, paper: SSC17-III-01, http://digitalcommons.usu.edu/cgi/viewcontent.cgi?article=3609&context=smallsat
54. Padmanabhan, S., T. C. Gaier, S. C. Reising, B. H. Lim, R. Stachnik, R. Jarnot, W. Berg, C. D. Kummerow and V. Chandrasekar, “Radiometer Payload for the Temporal Experiment for Storms and Tropical systems Demonstration Mission (TEMPEST-D),” In: Proc. 2017 IEEE International Geoscience and Remote Sensing Symposium (IGARSS 2017), Fort Worth, Texas, Jul. 2017, pp. 1213-1215.
55. Sara C. Spangelo, James Cutler, Louise Anderson, Elyse Fosse, Leo Cheng, Rose Yntema, Manas Bajaj, Chris Delp, Bjorn Cole, Grant Soremekum, David Kaslow, “Model Based Systems Engineering (MBSE) Applied to Radio Aurora Explorer (RAX) CubeSat Mission Operational Scenarios,IEEEAC Paper #2170, Version 1, Updated 29/01/2013, ” URL: http://www.omgsysml.org/mbse_cubesat_v1-2013_ieee_aero_conf.pdf
56. ESA Altimetry missions URL:https://www.esa.int/OurActivities/ObservingtheEarth/Copernicus/Altimetrymissions
57. ESA SAR missions URL: https://www.esa.int/OurActivities/ObservingtheEarth/Copernicus/SARmissions
58. Stacy N., 6U Radar Altimeter Concept, 6U Cubesat Low Cost Space Missions Workshop, Mt Stromlo Observatory, Canberra Australia, 17-18 July 2012
59. Wye L., SRI CubeSat Imaging Radar for Earth Science (SRI-CIRES), Earth Science Technology Forum 2016
60. Schiller, Q., Abhishek Mahendrakumar, with advisor Xinlin Li (2010), REPTile: A Miniaturized Detector for a CubeSat Mission to Measure Relativistic Particles in Near-Earth Space, 24th Annual AIAA/USU Conference on Small Satellite

61. Schiller, Q., Abhishek Mahendrakumar, with advisor Xinlin Li (2010), REPTile: A Miniaturized Detector for a CubeSat Mission to Measure Relativistic Particles in Near-Earth Space, 24th Annual AIAA/USU Conference on Small Satellites
62. Jim Cockrell, Richard Alena, David Mayer, Hugo Sanchez, Tom Luzod, Bruce Yost, D. M. Klumpar, "EDSN: A Large Swarm of Advanced Yet Very Affordable, COTS-based NanoSats that Enable Multipoint Physics and Open Source Apps," Proceedings of the 26th Annual AIAA/USU Conference on Small Satellites, Logan, Utah, USA, August 13-16, 2012, paper: SSC12-I-5, URL of paper: http://digitalcommons.usu.edu/cgi/viewcontent.cgi?article=1095&context=smallsat
63. "Edison Demonstration of Smallsat Networks Mission - A Swarm of Advanced, Affordable, COTS-based Nanosatellites that Enable Cross-Link Communication and Multipoint Physics," NASAFactsheet, URL: http://www.nasa.gov/sites/default/files/files/EDSN_FactSheet_031014.pdf
64. Adam Gunderson, David Klumpar, Matthew Handley, Andrew Crawford, Keith Mashburn, Ehson Mosleh, Larry Springer, James Cockrell, Hugo Sanchez, Harrison Smith, „Simultaneous Multi-Point Space Weather Measurements using the Low Cost EDSN CubeSat Constellation," Proceedings of the 27th Annual AIAA/USU SmallSat Conference, August 29, 2013, , paper: SSC13-WK-41, URL: http://digitalcommons.usu.edu/cgi/viewcontent.cgi?filename=0&article=2904&context=smallsat&type=additional
65. Brian Larsen, Harlan Spencer, David Klumpar, Larry Springer, J. Bernard Blake,"Focused Investigations of Relativistic Electron Burst Intensity, Range, and Dynamics (FIREBIRD)," CubeSat Developers' Workshop, CalPoly, April 22-25, 2009, URL: http://mstl.atl.calpoly.edu/~bklofas/Presentations/DevelopersWorkshop2009/2_Science/2_Larsen-FIREBIRD.pdf
66. David. M. Klumpar, Harlan E. Spence, Bernie Blake, "Overview: The Dual-CubeSat FIREBIRD Mission (Focused Investigations of Relativistic Electron Burst Intensity, Range, and Dynamics)," Nov. 30, 2009, URL: http://mstl.atl.calpoly.edu/~bklofas/NSF_comm/20091130_telecon/FIREBIRD_Overview_NSF_Telecon_113009.pdf
67. "The WINCS 'Factory' First of Many Miniaturized Helio Instruments to be Delivered this Fall," NASA, July 16, 2011, URL: https://www.nasa.gov/mission_pages/sunearth/news/wincs.html
68. DICE URL: http://www.sdl.usu.edu/programs/dice
69. Brent Sherwood, Sara Spangelo, Andreas Frick, Julie Castillo-Rogez, Andrew Klesh, E. Jay Wyatt, Kim Reh, John Baker, "Planetary CubeSats come of age," Proceedings of the 66th International Astronautical Congress (IAC 2015), Jerusalem, Israel, Oct.12-16, 2015, paper: IAC-15-A3.5.8
70. "Interplanetary Nano-Spacecraft Pathfinder in Relevant Environment (INSPIRE)," NASA/JPL, URL: http://www.jpl.nasa.gov/cubesat/missions/inspire.php
71. NASA Factsheet, URL: http://www.nasa.gov/pdf/467036main_OOREOS_FactSheet_FINAL_2010-10-29.pdf
72. Michael Schirber, "Outer Space Oreos", Space Daily for Astrobiology Magazine, Moffett Field CA (SPX) May 08, 2009 http://www.spacedaily.com/reports/Outer_Space_Oreos_999.html
73. Nathan E. Bramall, Richard Quinn, Andrew Mattioda, Kathryn Bryson, Julie D. Chittenden, Amanda Cook , Cindy Taylor, Giovanni Minelli, Pascale Ehrenfreund, Antonio J. Ricco, David Squires, Orlando Santos, Charles Friedericks, David Landis, Nykola C. Jones, Farid Salama, Louis J. Allamandola, Soren V. Hoffmann, "The development of the Space Environment Viability of Organics (SEVO) experiment aboard the Organism/Organic Exposure to Orbital Stresses (O/OREOS)satellite," Planetary and SpaceScience, Vol. 60, 2012, pp: 121–130, URL: http://www.gwu.edu/~cistp/assets/docs/research/articles/Ehrenfreund_SEVO_O-OREOS.pdf
74. NANOSAIL URL: https://www.nasa.gov/centers/marshall/pdf/484314main_NASAfactsNanoSail-D.pdf